Marine Geology 459 (2023) 107030

Contents lists available at ScienceDirect

Marine Geology

journal homepage: www.elsevier.com/locate/margo

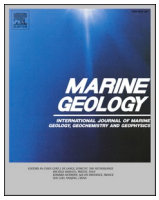

Sediment resuspension and transport processes during dense water cascading events along the continental margin of the southern Adriatic Sea (Mediterranean Sea)

Francesco Paladini de Mendoza [a,*], Katrin Schroeder [a], Stefano Miserocchi [b], Mireno Borghini [d], Patrizia Giordano [b], Jacopo Chiggiato [a], Fabio Trincardi [e], Alessandro Amorosi [c], Leonardo Langone [b]

[a] Consiglio Nazionale delle Ricerche-Istituto di Scienze Marine (CNR-ISMAR), Arsenale Tesa 104, Castello 2737/F, Venezia 30122, Italy
[b] Consiglio Nazionale delle Ricerche-Istituto di Scienze Polari (CNR-ISP), Via P. Gobetti 101, Bologna 40129, Italy
[c] University of Bologna, Department of Biological, Geological and Environmental Sciences, Piazza di Piazza di Porta S.Donato 1, Bologna 401269, Italy
[d] Consiglio Nazionale delle Ricerche-Istituto di Scienze Marine (CNR-ISMAR), Forte Santa Teresa, Pozzuolo di Lerici (SP) 19036, Italy
[e] Consiglio Nazionale delle Ricerche, Piazzale Aldo Moro 7, Roma (RM) 00185, Italy

ARTICLE INFO

Editor: Michele Rebesco

Keywords:
Cascading
Dense water
Adriatic Sea
Backscatter
Resuspension
Transport

ABSTRACT

The near-bottom nepheloid layer in the western margin of the Southern Adriatic Sea was monitored for 8-years by measurements acquired at two mooring sites. The two moorings, equipped with CTD probes and ADCPs, are located in the Bari Canyon and in an open slope sector along the Southern Adriatic Margin. These regions are of interest because affected by episodic dense shelf water cascading events whose dynamic has direct implications on deepwater morpho-dynamic, biogeochemical cycles and trophic networks. In this work, the sedimentation flux and its interdecadal dynamic is analysed examining in detail the sedimentary processes triggered by dense water flow through the analysis of the echo records of ADCPs.

The integration of hydrodynamic, turbidity and particle grain-size data provided estimates of the sediment flux, separating phases when the flow actively erodes the seabed from phases when particles are transported to the mooring location through density flows.

The frequency and velocity of dense-water cascading currents vary in time and space reflecting the capacity of sediment transport. Data analysis demonstrated that the hydrodynamic event that mostly accounts for sediment transfer to the deep basin is represented by current pulses induced by the passage of dense waters. The average annual sediment flux has been quantified and the Bari canyon shows transport more than five time larger than in the open slope sector, confirming that the canyon is the dominant pathway of sediment transfer to the deep basin. In contrast, in the open slope, albeit a minor lateral sediment advection, is impacted by currents that are able to trigger intense resuspension of seabed sediments, which can contribute over 80% of the total solid load.

This study allows unravelling the role of cascading in the sediment resuspension and transport processes and is essential to support deciphering the sedimentary records in the study area. The long temporal extent of the dataset used for quantification provides a reliable contribution to the Quaternary sediment budget determination.

1. Introduction

The Adriatic Sea is a Mediterranean sub-basin, characterised by shallow depths in its northern sector, and depths up to 1200 m in the southern sector, where the abyssal depression of the South Adriatic Pit (SAP) is located. Geographical position and surrounding orography expose this basin to north-easterly cold dry air masses, especially in winter, capable to trigger the formation of dense water (DW) masses through a combination of meteorological conditions coupled with oceanographic preconditioning factors, well described by Mihanović et al. (2013). Once DW masses are formed in the northernmost shallow sector, they flow southward along the western side of the Adriatic basin

* Corresponding author.
E-mail address: francesco.mendoza@ve.ismar.cnr.it (F. Paladini de Mendoza).

https://doi.org/10.1016/j.margeo.2023.107030
Received 27 October 2022; Received in revised form 12 March 2023; Accepted 18 March 2023
Available online 21 March 2023

following the isobaths (called North Adriatic Dense Water, NaDW). When DWs reach the shelf edge can cascade along the slope or are channelized offshore through submarine canyons until they reach their hydrostatic equilibrium (Canals et al., 2006; Pinardi et al., 2022). Cascading drives water renewal in the mid and deep ocean (Ivanov et al., 2004), ventilates the deep layer of the ocean even below the depth of ocean convection process (Pinardi et al., 2022) and are responsible of particulate matter transport with significant oceanographic and ecosystemic implications.

In the Adriatic Sea during the extreme cold air outbreak occurred in winter 2012 experiments have shown the dynamics of cold and DW masses along the shelf demonstrating the role of cascading events in the transfer of organic matter, playing a first- order control on the particulate flux transport (Langone et al., 2016). Geomorphological studies, (Foglini et al., 2016; Marini et al., 2016) have also demonstrated the impact of DWs on the seafloor and their active interactions with the pre-existing seafloor morphology. This process was recognized also in the western Mediterranean Sea off the Gulf of Lion, where dense shelf water cascading currents can reshape submarine canyons, transport large amount of sediment and organic matter to deep ocean playing a significant impact on deep-sea ecosystems (Canals et al., 2006; Palanques et al., 2006; Palanques et al., 2012). Other studies have recognized the morphodynamic implications due to the intense hydrodynamic field of cascading DW currents along continental edges at many sites around the world (Dong et al., 2017; Luneva et al., 2020; Mahjabin et al., 2020), but direct measurements are few and fragmented.

Along the continental slope of the Southern Adriatic Margin (SAM) (Fig. 1) moorings have been deployed and continuously recorded thermohaline and hydrodynamic properties through an array of probes deployed along the water column. Two of these moorings are still active and are located, in the main branch of the Bari Canyon and in the open slope off the Gargano Promontory in a furrowed area characterised by numerous and well-defined lineations defining regularly spaced furrows on the seafloor (Flood, 1983) described by Verdicchio and Trincardi (2006); Verdicchio et al. (2007) and Foglini et al. (2016).

The continental slope is a transitional zone between the continental shelf and the deep basin where sediment particles eroded on land are dispersed and may be affected by several transport, deposition and resuspension cycles. On the continental margins the submarine canyons generally enhance seaward sediment transport, acting as a preferential route for the shelf-slope exchange of particles toward the deep-sea (Allen and Durrieu de Madron, 2009; Canals et al., 2006). The particulate transfer dynamics of canyon systems is strongly influenced by the distance from nearshore sediment supply from rivers and wave energy (Palanques et al., 2005a; Xu et al., 2002; Palanques et al., 2005b; Martín et al., 2006; Liu et al., 2002; Harris et al., 2003; Puig et al., 2003).

In the Adriatic Sea, the Bari Canyon System (BCS), although far from the present-day coastline, has remained active during sea-level rise and the actual high-stand sea-level condition (Trincardi et al., 1995, Trincardi et al., 2007a). It represents an efficient conduit delivering suspended sediment from the continental shelf to the deep southern Adriatic basin.

In this study, the Sediment Flux (SF) in two sites along the continental slope of the south-westerm Adriatic margin is analysed trough turbidity and acoustic records of Acoustic Doppler Current Profilers (ADCPs) deployed on the moorings.

ADCPs, commonly used to measure current profiles can be used also to evaluate the suspended materials by means acoustic backscatter intensity signal (Reichel and Nachtnebel, 1994; Thevenot et al., 1992). This approach is particularly used in estuaries and bay systems (Gartner, 2004; Longdill and Healy, 2007; Murphy and Valle-Levinson, 2008; Shi et al., 2006; Yuan et al., 2008), while in the open ocean these applications are more oriented to study zooplankton dynamics (Wade and Heywood, 2001; Guerra et al., 2019). The backscatter signal can indeed be used also to extract information on the scatterers (Holdaway et al., 1999). It provides non-intrusive estimates of suspended materials in parallel with current field velocities, through the water column in definite layers and being less susceptible to bio-fouling, makes this method advantageous relative to the traditional measurement techniques. The limitations of this approach are mainly related to the variability in backscatter response that depends on the size of the reflectors and the acoustic frequency of the instrument (Lohrmann, 2001). Optical and acoustic measurements differ also for the volume of water sampled and can vary significantly with respect to particle concentration and acoustic properties which depend on particle size, composition, and shape (Lynch et al., 1994). Acoustic backscatter is particularly sensitive to large particles, and this often causes difficulties in correlating with optical backscatter instruments that are more sensitive to fine particles

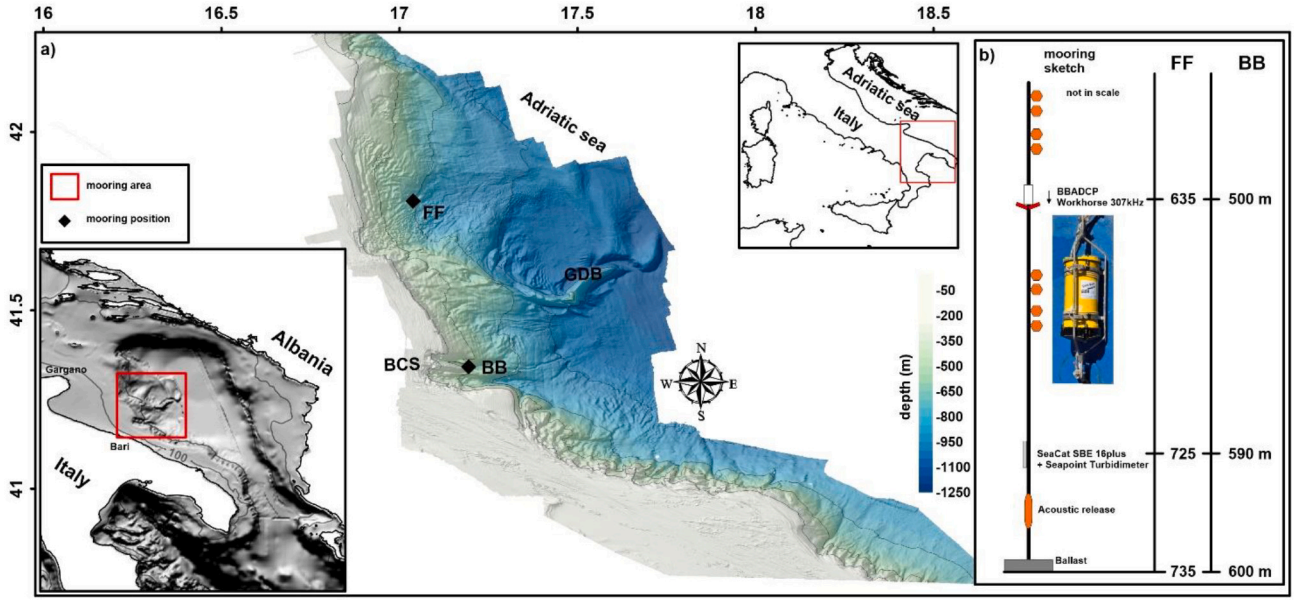

Fig. 1. (a) Study area and digital terrain model (DTM) of the western sector of the Southern Adriatic Margin (SAM); (b) sketch of the moorings' structure, FF (open-slope) and BB (canyon) are the two mooring names and in the pictures is shown the ADCP-Workhorse mounted on the mooring. The depths shown as metres water depth.

(Gentil et al., 2020). However, previous studies have shown both concordance between the two measurements especially if the sediment is uniform (Lynch et al., 1994; Lohrmann, 2001) but also complementarity between the methods when populations of particles of different sizes are present (Glenn et al., 2008; Gentil et al., 2020).

The aim of this work is to estimate the near-bottom (approximately 100-m layer) SF at two sites along the continental slope during the period from 2012 to 2020 focusing on the role played by DW cascading events on sediment dispersal. SF during the most intense phase of DW passage is define also through a section by exploiting the ability of ADCPs to insonify with high resolution a wide portion of water column. Ancillary sedimentological information was additionally used to evaluate when the near bottom dense flow can trigger in-situ resuspension. The analysis conducted allows defining the role of cascading events on the total sediment budget and its spatial variability, giving a quantitative assessment of erosional and transport capacity of modern sedimentary processes affecting the continental margin. Encompassing nearly a decade, our reconstruction of the temporal variability of recent fluxes provides insight on the role of such process in building the sedimentary record on geologic time scale.

2. Study area

The SAM was built during the last half million years in response to high frequency eustatic depositional cycles coupled to complex deformation processes (Ridente et al., 2007; Trincardi et al., 2007; Foglini et al., 2016). The shelf edge is rectilinear and erosional north of Bari and becomes more irregular proceeding southwards where the slope is dissected by gullies and canyons (Fig. 1). Along the continental slope two moorings (BB and FF) were positioned in two locations, known as key passage of DWs (Chiggiato et al., 2016b).

The BB mooring is positioned in the northern straight arm of BCS, the main conduit for off-shelf flows (Trincardi et al., 2007a, 2007b). This narrow, straight, symmetrical incision has a slope of about 5% up to 400 m depth and gentler between 500 and 600 m depth. The seabed morphology shows bottom current activity (Verdicchio et al., 2007; Bonaldo et al., 2016) ascribed to the interplay of two main water masses: the Levantine Intermediate Water (LIW), and the NAdDW currents (Verdicchio et al., 2007; Trincardi et al., 2007b). The *E*-W southern arm of the canyon is instead broad in the shelf edge region and very asymmetrical in its deepest reaches with a very steep right-hand flank.

Previous oceanographic observations (Chiggiato et al., 2016a) conducted during the DW cascading event of 2012, highlight in the two arms of BCS bottom currents with the same profile in the 40mab (meter above the bottom) layer. In shallower levels a geostrophic flow is observed in the northern channel (where BB is located) while an along axis current characterizes the southern channel. Such behaviour in the southern channel indicates canyon wall forcing DW transport (Wåhlin, 2002; Jiang and Garwood, 1996). However, the average bottom velocities measured by current meters in both arms of BCS were remarkably similar. The study of BCS growth (Trincardi et al. 2007) from the LGM made it possible to define the main trajectory of the DW currents entering through the upper segment of the north channel, which is straight, narrow and steep, and subsequently flowing over its right bank at about 600 m depth, where the bank relief on the channel bottom is minimal and entering the south channel where substantial erosion takes place. The upper portion of the South Canyon, has hard grounds and corals indicative of a reduced influence of sediment-ladent currents, while its lower portion, where occur deep-sea furrows with NW-SE orientation, collects additional flows from the upper North Channel.

Although mass flux in the canyon is greater than on adjacent slopes, cascading dense-shelf waters impact the entire South-western Adriatic margin. Numerical simulations and geo- morphological analysis have defined the main pathways and geometric characteristics of DW both on the shelf and along the Adriatic shelf break (Rubino et al., 2012; Chiggiato et al., 2016a; Foglini et al., 2016; Bonaldo et al., 2016; Rovere et al., 2019), with a significant component of DWs remaining on the continental shelf and shaping erosional features and large scale bedforms (Rovere et al., 2019). Mooring FF is located in an open slope region where the flow is concentrated in areas north of Bari Canyon within a region sculptured by abyssal furrows, between 550 and 750 m (Verdicchio et al., 2007), with length, width and spacing of 1–11 km, 20–100 m, 100–200 m, respectively, witnessing occasionally strong and directionally persistent currents (Trincardi et al., 2007a). Their orientation of about 145°N agrees with the direction of cascading DW currents, as observed from extended hydrodynamic records from 2012 to 2020 (Chiggiato et al., 2016a, Paladini de Mendoza et al., 2022a). Along the open-slope the vein of DW proceeding toward FF site initially showed a thickness of about 20 m on the shelf and then doubled as it descendent on the slope, with an active layer up to 40 m thick due to ambient water entrainment (Chiggiato et al., 2016a). DW flows down the slope are very efficient in mixing the original NadDW with ambient water (Chiggiato et al., 2016a) in fact, the observed thickening is consistent with the change in temperature (T) from 12 °C to 12.8 °C, considering mixing with ambient T of 13.8 °C.

3. Materials and methods

The data come from the two moorings equipped with an ADCP and CTD positioned along the continental slope of the Southern Adriatic Sea (Fig. 1). The site called BB is in the axis of the main branch of BCS at 41°20.456′N, 17°11.639′E whereas the site FF is placed at 41°48.396′N, 17°02.217′E on a furrowed area of the continental slope. The moorings' structure represented in Fig. 1b are 110 m long moorings, on which a series of oceanographic probes and profilers are mounted at different depths. The downward facing ADCP systems measure the velocity and direction of currents through the water column and have a T sensor in their transducer head; CTD probes measure T and salinity at 10 m above the seafloor. The mooring deployments were from March 2012 to June 2020 and are divided in separated deployments, each of an approximate duration of 6 months, to allow for mooring turnaround, data downloading and maintenance. The methodology has the goal to estimate the SF focusing on the role of cascading events using backscatter measurements to separate the resuspended to the transported fraction. This purpose is achieved by exploiting the ADCP's ability to make high resolution measurements through the water column and by relating them to the other measured oceanographic variables. The physical data of T and potential density anomaly (σ) are a robust trace of the passage of DW that can be related to the hydrodynamic field and backscatter as well as turbidity data are used to validate the backscatter signal.

3.1. Sedimentological analysis

The sedimentology of the mooring sites was determined through analysis of seabed samples collected during various surveys between 2011 and 2014. Samples from the Bari Canyon were collected during two oceanographic cruises in 2011 (OBAMA 11, Langone, 2011) and 2014 (SIRIAD 14) by means of a box corer and 60 L Van Veen grab by multiple deployment. The box-corer (internal diameter 32.4 cm) was equipped with a closing lid by which the original bottom water is retained above the sediment-water interface and disturbance of the sediment water interface is minimized. The sample from the FF site on the open slope was collected during the ADX14 oceanographic cruise of 2014 (Lopes-Rocha et al., 2017) using a mini box corer. Samples were refrigerated on board at 4 °C and an aliquot of sediment was dried at 60 °C and homogenized for sediment characteristics. Grain size was determined after the removal of organic matter by H_2O_2 and wet sieving at 2 mm and 63 μm to separate coarse fraction (gravel and sand) from fine fraction (silt and clay).

3.2. ADCP data

The ADCPs used are broadband systems of the type RDI Workhorse (Teledyne RD Instruments USA, Poway, California), with a four-beam, convex configuration, a beam angle of 20°, and a frequency of 307 kHz. The water profiling for the used system with a depth cell size set to 4 m has a range of 103.66 m and a standard deviation of 0.5 cms^{-1} for an ensemble of 50 water pings. The currents velocity can be determined with an accuracy measurement of ±0.5% of the water velocity relative to the ADCP ±5 mms^{-1} and the resolution of 1 mms^{-1}. The tilt and compass sensors have an accuracy of ±0.5° and ± 2° respectively, a precision of 0.5° and a resolution of 0.01°. The echo intensity profiling has a vertical resolution dependent on the depth cell size, a dynamic range of 80 dB and a precision of ±1.5 dB.

An ADCP computes sound speed based on an assumed salinity and transducer depth and on the T measured at the transducer (range between −5° to 45 °C with a precision of ±0.4 °C and resolution of 0.01 °C). The instruments are moored at a nominal depth of 500 m and 600 m, at BB and FF, respectively, in a downward-looking mode, at roughly 100 m from the seabed. All current data are made publicly available from doi:https://doi.org/10.5281/zenodo.6770201 (Paladini de Mendoza et al., 2022b) while echo intensity data are made publicly available from doi:https://doi.org/10.5281/zenodo.7586134 (Paladini de Mendoza et al., 2020). All details about settings, deployments and quality control procedure are described in Paladini de Mendoza et al. (2022a).

3.3. Shear stress determination and sediment motion

To predict sediment motion and relative transport it is necessary to relate the frictional force exerted by the fluid and consequent bed shear stress. The bed shear stress of the current flow can resuspend the seabed sediment when it exceeds the critical threshold for the start of motion. The bottom shear stress and critical velocity for a defined cohesion-less sediment class is derived from the current velocity data using simplified formulae, assuming a flat bed and current-only bottom boundary layer (Madsen and Wood, 2002) detailed in the Appendix A.

The sedimentological information about the composition of the bed sediments in the mooring areas indicate a sediment mixture of sand and mud, (detailed in next section 4.1). For cohesionless sand class the critical velocity is derived from the equations of Madsen and Wood (2002) and determine the onset of resuspension during flow pulses, giving the value of 0.36 ms^{-1} for a fine-sand grain diameter of 0.2 mm, which represents a mean grain size (D_{50}) for the SAM bedforms (Rovere et al., 2019). Regarding the mud component (D < 63 μm), the strength of particle cohesion is a very important parameter and using literature formulations can produce too much uncertainty. For this reason, we refer to laboratory flume experiment observations of Schieber et al. (2010), where erosion experiments under an increasing current speed were conducted on clay-bed with different rates of consolidation. These experiments were designed to allow for a closer approximation to transport and flow conditions in natural environments. From the experiment observations we considered the results obtained from the most consolidated bed-sediment composed by mud bed deposits (D < 63 μm) obtained after 9 weeks of consolidation that showed first signs of erosion starting from 0.16 m s^{-1}, without sensitive change in turbidity, while from 0.26 m s^{-1} onwards Suspended Sediment Concentration (SSC) quickly climbed with a continuous sustained erosion. We considered the threshold of 0.26 m s^{-1}, because determining a real change in turbidity level, might have stronger correspondence with our observations of acoustic backscatter variations.

3.4. Backscatter determination

Acoustic backscatter strength can be used to estimate the concentration of suspended sediment and zooplankton in Broadband ADCPs, starting from the Echo Amplitude signal (*E*). Many different formulations exist to estimate backscatter from *E* of acoustic beams. When the bulk of backscattering particles are of sedimentary nature, the acoustic intensity can be used as a proxy for total suspended solid concentration of the water column. The formulation proposed by Deines, 1999, is one of the most frequently referenced papers. Recently, Mullison (2017) reviewed the formulations and proposed a revised formulation which has the advantage to better resolve the signal and the noise and to retain the behaviour also in a low backscatter environment with general low-concentration of suspended matter such as in our case of pelagic environments.

The formulation used in this study (fully detailed in Appendix B) to determine backscatter for every depth cell is composed of signal and noise terms, plus other terms that depend on the broadband ADCP system used, oceanographic conditions and sampling strategy.

3.5. CTD and Turbidity data

Attached to the mooring at both stations at approximately 10 m above the seabed there is a CTD probe, SBE 16plus V2 SeaCAT to record oceanographic parameters. Data of water conductivity was measured by sensor, with accuracy of 0.0005 S/m and resolution of 0.00005 S/m; the water T by means of a thermometer, with accuracy of 0.005 °C and resolution of 0.0001 °C; the water pressure by means a pressure strain gauge sensor with an accuracy of 0.002% of full-scale range. The σ is automatically calculated during data conversion with SBE-Data Processing software. All CTD data are made publicly available from doi: https://doi.org/10.5281/zenodo.6770201 (Paladini de Mendoza et al., 2022b) and for Turbidity from doi:https://doi.org/10.5281/zenodo.7586134 (Paladini de Mendoza et al., 2023). All details about settings, deployments and quality control procedure are described in Paladini de Mendoza et al. (2022a).

The probe is also equipped with a Seapoint Turbidity Meter that measures turbidity by detecting scattered light from suspended particles in the water. The used sensor has a light source wavelength of 880 nm and confines the sensing volume to within 5 cm of the sensor in a scattering angle between 15° and 150° where the peak sensitivity is at 90°, allowing near-bottom measurements and minimising errant reflections in restricted spaces. It measures turbidity trough a linear relation of the response in Formazin ±2% in a range between 0 and 25 FTU with a sensitivity of 200 mV/FTU. The turbidity measurements are differently available in the two mooring sites. In BB measurements are available from March 2012 until June 2020 while in FF from June 2012 until May 2018.

3.6. Determination of solid load transport during cascading events

At the mooring sites, ADCPs provide acoustic measurements of a 100-m-thick near-bottom layer, with high temporal and spatial resolutions that allow determination of currents and backscatter. Simultaneous determination of particle concentration from the turbidimeter, backscatter and currents allow calculation of particle SFs during the monitoring period and during the passage of DW currents that cascade along the continental slope.

Instantaneous Flux (IF) of suspended sediment is calculated for each time step from the product of current velocity and SSC (mg L^{-1}). The Cumulative Flux is calculated by summing the IF multiplied by the time-step. The calculation was conducted on both ADCP backscatter data and turbidity sensor measurements. In the ADCP data, the IF in each depth-cell is determined, allowing the vertical variability of the flow to be considered. Once backscatter is determined, as explained earlier, it is converted to turbidity (FTU) using the relations found between backscatter in the same depth cell as the turbidity sensor at the two mooring sites. The average backscatter of the four ADCP beams is used, because the turbidity sensors were not collocated within any of the beams (Gartner, 2004). The transformation from turbidity unit (FTU) to SSC is

complex and a general conversion factor does not exist. Each instrument for each environment should have a specific calibration curve. In the Mediterranean Sea field calibrations are scarce and complicated to carry out, especially when the sensor is at 500–600 m depth. The difficulty of proper calibration is compensated by the use of the equation proposed by Guillen et al. (2000) (Eq. (8)), which represents an average relation usable to retrieve SSC (in mg L^{-1}) for semi-quantitative purposes.

$$SSC = 1.74\ FTU - 1.32 \quad (8)$$

DW currents that cascade along the slope can actively resuspend the bed sediments and transport particles exported from the shelf. For the ADCP data, time series is screened in detail and portions of the dataset with evident signatures of cascading processes are selected out. The selection does not allow grouping all DWs passage events in the study area, but only those phases when the process is intense enough to produce evident backscatter, hydrodynamic, turbidity and thermohaline signals. To determine the hydrodynamic conditions able to promote sediment erosion the module of current velocity at the bottom is considered by relating it to the critical velocity threshold for the for the two representative particle size fractions (defined in section 3.3), in order to separate the hydrodynamic conditions favourable for resuspension and those favourable for transport conditions. During resuspension conditions, particles are actively eroded in situ and then transported along the slope, while during transport conditions the currents are not intense enough to actively erode the seabed, but may only transport the eroded particles elsewhere within the dense flow. The Fig. 2c represents the two components of the flux on the basis of the bottom current speed.

Acoustic observations provide high vertical resolution of water mass dynamics, while turbidimetric measurements provide information limited at a given elevation. SF at the two sites was calculated through two sections considering the current component perpendicular to them as shown in Fig. 2a, b. At FF slope strike is on average 170°N, thus the cross-isobath perpendicular orientation is 80°N and include a 22-km long slope sector where the increase in slope is observed, as explained in section 2, in which the transit of dense currents is favoured (Chiggiato

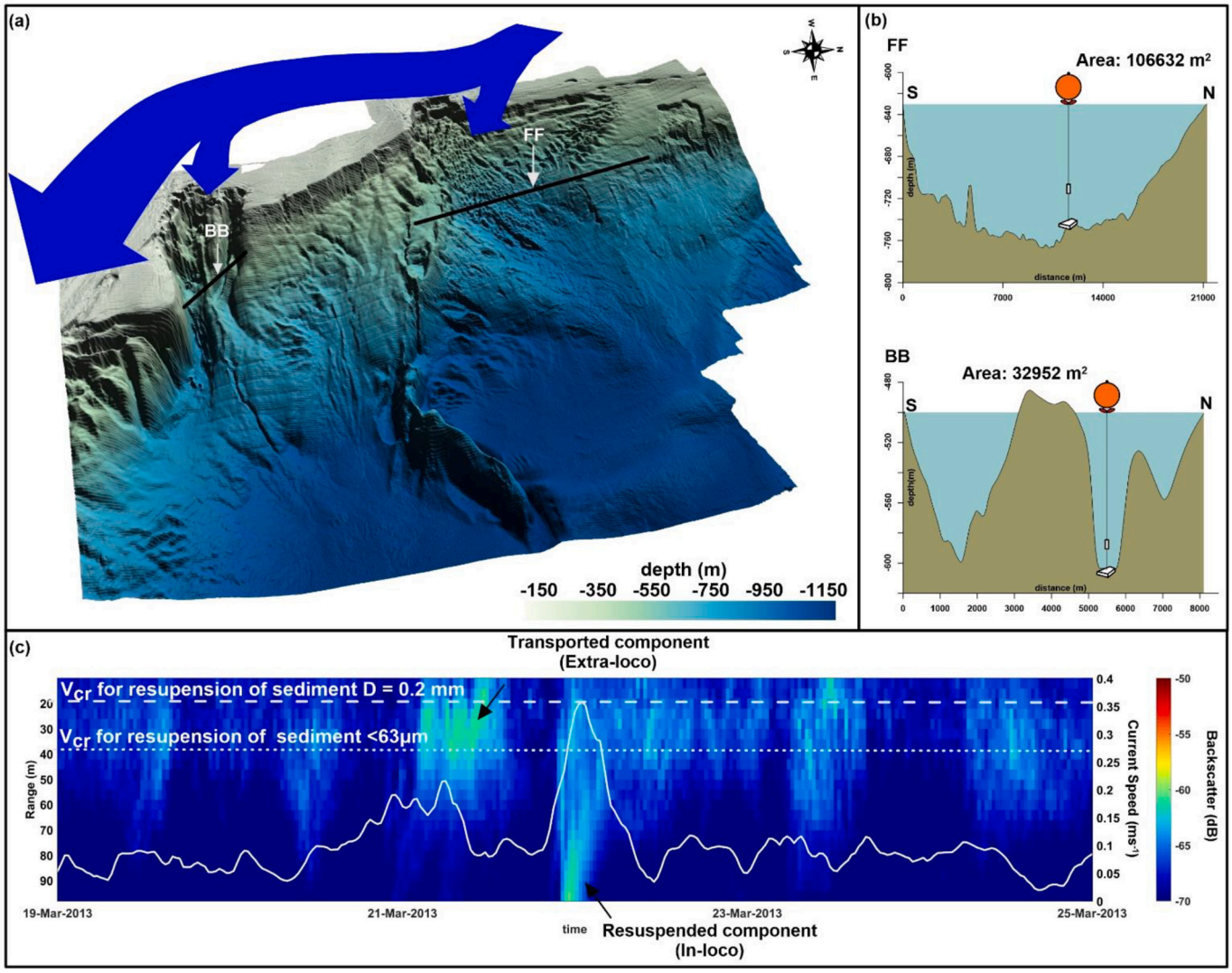

Fig. 2. (a) Scheme of the DW cascading dynamics along the continental slope. The arrow orientation representing the cascading flow along the open slope and the canyon correspond to the real measured direction. (b) Sections along the slope extracted from the DTM through which the solid transport caused by cascading events was calculated (the value of the section area is relative to light blue filling). (c) Representative plot of sedimentary processes. The white line indicates the bottom current velocity in relation to the critical threshold speed of resuspension (current velocity in ms^{-1}) of sandy (D = 0.2 mm) and mud fraction sediment particles (D < 63 µm) indicated by the dashed and dotted white lines, respectively; The distribution of backscatter is colour-coded, and the arrows indicate the signal attributable to the resuspension of locally resuspended particles (in-loco) from the bottom and to particles transported into the dense flow from outside the local area (extra-loco). (For interpretation of the references to colour in this figure legend, the reader is referred to the web version of this article.)

et al., 2016a), which through high-energy pulses cause the formation of abyssal furrow marks (Verdicchio et al., 2007). The perpendicular to the section through BB is oriented along the canyon axis (110°) and extends for about 8 km between the two edges of the BCS. As explained in section 2, the hydrodynamic measurements showed similarity of mean bottom current velocity and the southern edge represents a constraint forcing dense flow within the canyon.

As for the acoustic data, the sections have the water column layer observed by the ADCP as the vertical extent. As shown in Fig. 2b, the actual area of the section was defined cartographically by the DTM of Fig. 1a. The canyon section covers 32,952 m^2, while the open slope section covers 106,632 m^2.

The calculated SF in each cell is integrated along the water column and multiplied by the area of the section determining an estimate of the SF produced by the cascading events in the two morphological units (Fig. 2b).

The obtained solid load is then compared with previous estimates (Frignani et al., 2005; Lopes-Rocha et al., 2017) conducted at the same site with similar estimates in other sites of DW passage (Palanques et al., 2006, 2012).

3.6.1. Sediment flux determination

The SF is derived from measurements affected by random and systematic errors which produce uncertainty. Following the approach of Durrieu de Madron (2019) used for the determination of propagation of uncertainty on parameters derived from time series we have considered the uncertainties produced by random errors of each parameter that enter in the SF calculation. Considering the determination of the SF:

$$SF = V \times SSC \tag{9}$$

The uncertainty(σ_F^2) is determined by the function:

$$\sigma_F^2 = \left(\frac{\partial F}{\partial V}\right)^2 \times \sigma_V^2 + \left(\frac{\partial F}{\partial Dir}\right)^2 \times \sigma_{Dir}^2 + \left(\frac{\partial F}{\partial FTU}\right)^2 \times \sigma_{FTU}^2 \tag{10}$$

Where σ_V, σ_{Dir}, σ_{FTU} are respectively the errors of the current speed, current direction and turbidity. In the determination of the SF obtained from the ADCP data through the backscatter the FTU uncertainty is substituted by turbidity error obtained from the fitting of turbidity and backscatter (σFTU_{BS}). In the Table 1 are resumed the errors considered for the different parameters.

4. Results

4.1. Sedimentological asset

The results of sedimentological analysis are summarised in Fig. 3, reporting sampling locations and the textural composition of samples close to the mooring sites. . Numerous samples collected along the Bari canyon provide a comprehensive overview of sedimentological characteristics of the BB mooring site, while for FF only one sample was available. Samples closest to the mooring location show for station BB a fine fraction percentage between 26% (OB11-BC1) and 50% (48–609) while at station FF this represents 42%. An underestimation of the fine fraction is possible in sample OB11-BC1 which having been collected by grab implies an under-sampling of the fine fraction. Grain-size analysis from the canyon (Fig. 3c) showed increasing percentages of mud with increasing depth. The heads of both channels present reduced mud occurrence and a dominance of coarse grain material. Sand proportion from the northern channel, where BB is located, ranged between 49 and 70%. The highest mud percentage was instead recorded at the confluence of both channels and in the moat, out of the northern channel. In the open slope region, where FF mooring is placed the sand content is 57%.

Table 1
Error value used for parameters considered in the calculation of SF.

Parameter	Value
σV	0.005 [ms^{-1}]
σDir	2°
σFTU	0.5
σFTU_{BS}	2.63 (BB) – 0.4 (FF) [FTU]

4.2. Dense water cascading events

The time-series between 2012 and 2020 highlight temporal variations of thermohaline properties. In Fig. 4 T drops in T of variable intensity recur annually, accompanied by increasing σ in the lower layer (red line) recording the passage of DWs. During the passage of DWs, the T drops below the mean value of 13.9 °C in BB and 13.6 °C in FF (Paladini de Mendoza et al., 2022a) depending on the intensity of the event and can reach values below 12.5 °C during the most intense ones. T variations are more evident in BB and clearly appreciable in both layers. Otherwise, in FF, T variations are less pronounced and more marked in the lower layer. The passage of these DWs is not recorded every year, but clearly occurred during 2012, 2017 and 2018. In BB site, although less marked, it is also recorded in 2019.

The polar diagrams of Figs. 5 show the linkage between the hydrodynamics and T (Fig. 5a) and σ (Fig. 5b) data. In BB the currents flow in two main directions (south and south-east) with accelerations concentrated at the bottom. The most intense currents characterise the passage of the densest water masses and flow south-east nearly along the canyon axis.

In FF, the dense and cold current pulses involve a thin near-bottom layer and are directed south-eastward. These DW masses that cascade along the slope are thus characterised by physical features and represent a small portion of the observations which are generally characterised by a weak hydrodynamic field (speed <0.1 ms^{-1}). The most intense thermohaline variations are observed in 2012 and 2018 in both sites with maximum value of σ in a range between (29.35–29.51 Kgm^{-3}) where the maximum is reached in the FF site (Fig. 5c). In Fig. 5c these values were compared with the σ recorded in the same years between January and May in the southern Adriatic basin from Argo float CTD profiles (retrieved from Coriolis database - https://dataselection.coriolis.eu.org/) showing that the cascading currents have a σ noticeably larger than the maximum value observed below 700 m (29.01–29.08 Kgm^{-3}) in the basin water masses.

Simultaneous screening of these thermohaline and hydrodynamic variations that characterise the DW passage along with the occurrence of turbidity and backscatter signals related to particulate movement were used to select cascading events from the whole dataset. The result of this selection is shown in Table 2, and these events were then used for subsequent computations of SF using backscatter data. At site BB they represent a frequency between 0.54 and 5.75%, while at site FF their frequencies fluctuate between 1.91 and 11.5%.

The selected events are shown with a higher level of detail in Figs. 6 and 7, where each panel represents a specific event. Turbidity records are not available for the 2012 event in FF and from the 2018 event in BB. In terms of vertical variability, the two sites are markedly different, as also observed in Fig. 5: in FF thermohaline variations and current pulses concentrate near the bottom, turbidity is higher in BB than in FF and the backscatter signal has an evident vertical gradient in BB, testifying to higher concentration of particles in the water column. The signal near the bottom is generally less pronounced, with the exception of periods when velocities are intense enough to actively resuspend the bottom sediment. In BB variations in backscatter and turbidimeter records are not always synchronous with current pulses and T fluctuations. In FF, on the other hand, the current speed impulses and T variations match those of turbidity and backscatter along the water column and are more concentrated at the bottom, especially during the peaks of near-bottom currents.

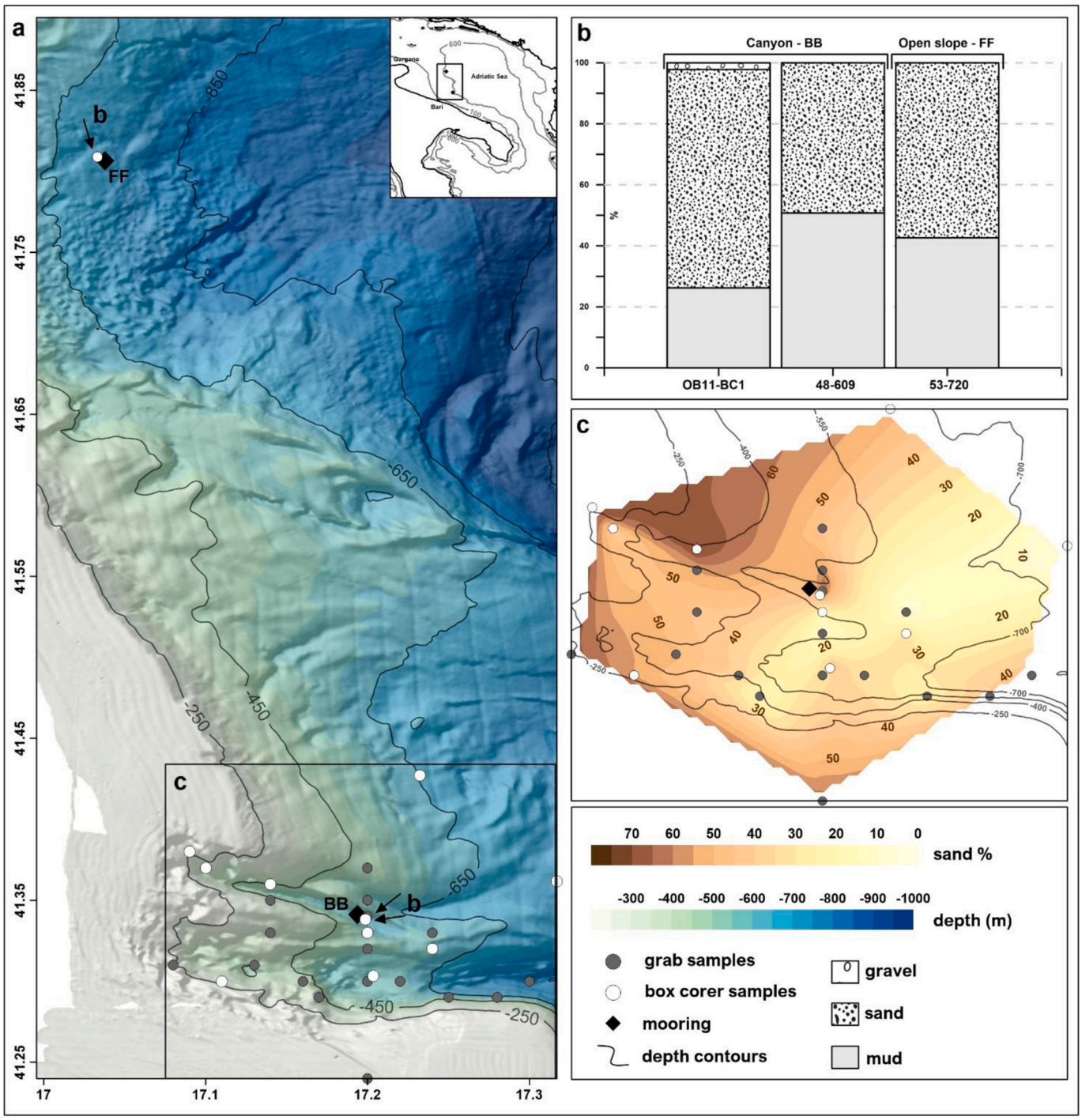

Fig. 3. Morphology and sedimentology of the mooring sites; a) Digital Elevation Model of the South Adriatic Margin (SAM), mooring position (black diamonds) and sediment samples positions (grey and white circles respectively for grab and box-corer samples), the black arrows indicate the samples used to represent the site sedimentology in panel b; b) Grain-size composition of bed sediment in the two sites (refers to the samples indicated by arrows in the map a; note that in the canyon the sample 48–609 is collected by box-corer while OB11-BC1 by grab; c) percentage distribution of sand in the Bari Canyon.

The turbidity at 10 mab and backscatter measured at the same depth (light grey and black lines in panels b of Figs. 6 and 7, respectively) were plotted together and analysed through regression (Fig. 8). The analysis found a significant exponential relation between backscatter and turbidity with $R^2 = 0.62$ and RMSE = 2.63 for BB (Fig. 8a) and $R^2 = 0.7$ and RMSE = 0.39 for the FF site (Fig. 8b). The two equations found from the two regressions were used to convert backscatter signals in the turbidity unit (FTU), extending the data acquired only at a certain depth on the insonified water column (approximately last 100 m).

4.3. Near bottom sediment flux

The results of the near-bottom SF estimation are represented in Fig. 9a (BB) and 10a (FF) where the IFs show a predominantly down-slope orientation at both sites with peak fluxes between 4 and 15 g^{-2} s^{-1} and particularly in the FF section the up-slope contribution appears particularly low. In Figs. 9b and 10b the cumulative curve representing the down-slope SF has a dynamic characterised by a few major events that have a primary influence on the total contribution and that recur

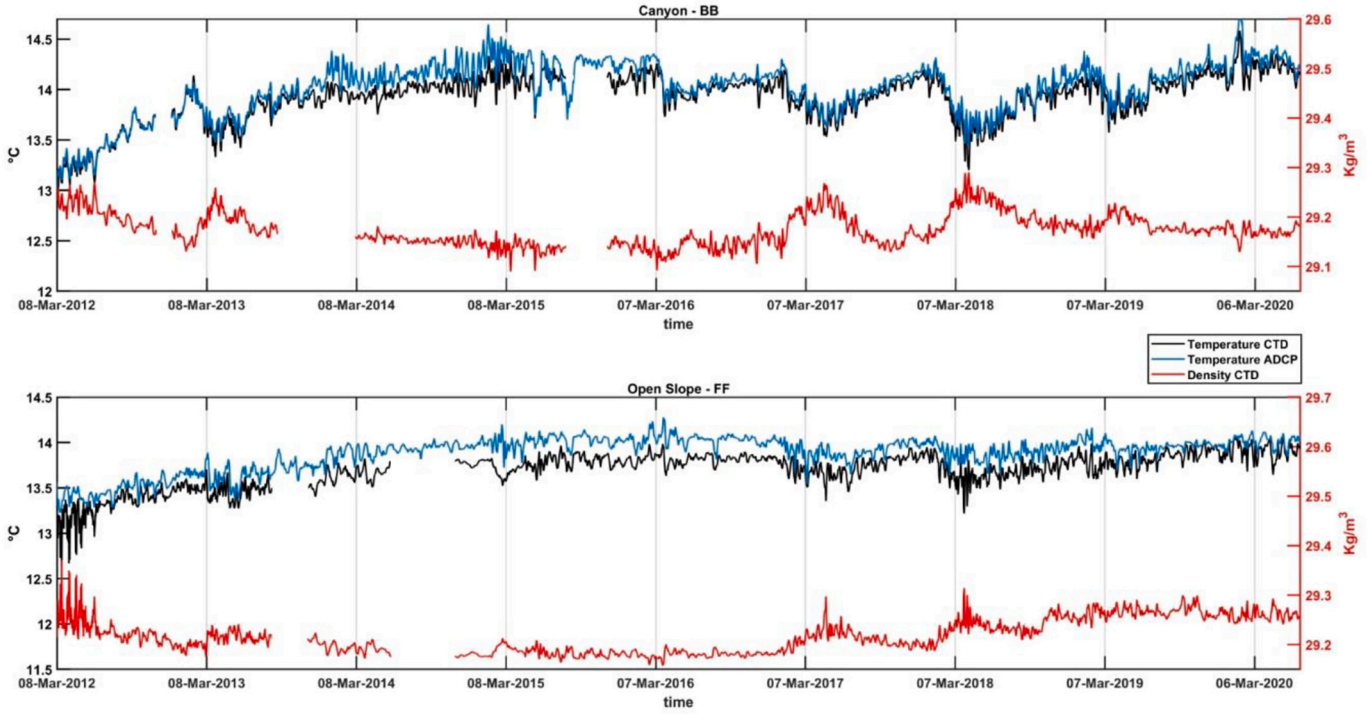

Fig. 4. Time-series smoothed with a 7-days window of T and sea-water σ records at 100 m(blue) and 10 m (black) above the seabed. The σ is obtained from CTD records at 10 mab. (For interpretation of the references to colour in this figure legend, the reader is referred to the web version of this article.)

mainly in the period between February and May, but variably over the years. At site BB the cumulative downslope flux between 2012 and 2020 was 55,636±52.77 Kgm^{-2} while at site FF from 2012 to 2018 the total flux was 6868±25 Kgm^{-2}. The determination of the down-slope fluxes at sites BB and FF has a total relative error of 0.09 and 0.36%, respectively.

Compared to the down-slope component, the up-slope component contributes less to the total budget indeed this component (not shown in the cumulative graph of Figs. 9b and 10b) amounts to 4960 Kgm^{-2} in BB and 382 Kgm^{-2} in FF, representing a contribution of <10% (8.2% BB and 5.2% FF) of the total flux through the two sections. The annual SF at the BB site exhibits an oscillation with minima in 2015 (168±0.3 Kgm^{-2}) and highs in 2017 (15,554±10 Kgm^{-2}) (Fig. 9b). At the FF site (Figs. 10b), the annual SF fluctuates between minimum values in 2014 (10±0.06 Kgm^{-2}) and maximum values in 2018 (2583±5.2 Kgm^{-2}). In both sites, the years when the SF was highest were 2012, 2013, 2017 and 2018 and their sum represents 80% of the total solid contribution in BB and 98% in FF.

4.4. Sediment flux estimated from backscatter during cascading events

The backscatter derived IF, integrated along the water column observed by ADCP in the two sites during cascading events is represented in Figs. 11 (BB) and 12 (FF). In the panel *a* of both figures, the velocity of bottom currents, highlighting the sedimentary processes that take place depending on the bottom current speed and the resuspended and transported components are separated to evaluate the relative contributions on the total SF.

In the panel *b*, in addition to the total SF produced by each event is also represented the estimation of resuspended and transport fraction. In BB, the IF is the largest and the peaks range between 22 and 120 $g^{-2}\,s^{-1}$. The cumulative flux obtained from each selected event ranges between the maximum of 11,280 and 462 kgm^{-2} with a total value of 21,741±71 Kgm^{-2}, with a relative error of 0.32%. Within the flow, the transport component ranges from 9% to 95%, and resuspension contributes from 5% to 91% of the total load, with a dominance of the mud fraction. The most intense event was recorded in 2018, when bottom currents exceeded 0.6 ms^{-1}, with a significantly greater contribution from the resuspended sand and mud component (82%) than in other years (0.3–37%). A cascading event was also recognized at this site for the year 2019, while in FF the backscatter signal did not produce clear signals of increased suspended solid along the water column.

In FF, the depth-integrated IF produced by the cascading events has peaks ranging from 8 to 68 $g^{-2}\,s^{-1}$. The cumulative flux of each selected event ranges between 85 and 4021 Kgm^{-2} with a total value of 11,030 ±15 Kgm^{-2}, with a relative error of 0.13%. Within the SF, the transported component ranges from 21% to 55%. In general, the resuspended component in FF is always abundant, and varies between 43% and 77%, >60% is composed of sand and mud. The most intense events were recorded in 2012 and 2018, when currents reached velocities >0.7 ms^{-1} (Figs. 7 and 12), with a large production of resuspended material (69–77%).

5. Discussion

5.1. Characteristics of dense water cascading events

The thermohaline time-series 2012–2020 (Fig. 4) shows a clear seasonality of the passage of DW masses, in late winter and early spring (of some years), and is characterised by a marked interannual variability (Paladini de Mendoza et al., 2022a) as observed in previous (shorter-term) experiments (e.g., Turchetto et al., 2007). The temporal variability is accompanied also by an evident spatial variability, with the two mooring sites, on the open slope and in the narrow canyon behaving quite differently. During the DW passages, thermohaline and hydrodynamic properties vary together. In the canyon DWs pulses invest a thick layer of the measured water column, despite being more distinctive near the bottom. On the open slope, instead, DW are visible only near the seafloor (Figs. 4 and 5) as trains of short-lived pulses (Fig. 7) oriented toward south-east, when bottom currents reach their maximum velocity. In BB the maximum velocity of currents is comparable, but the pulses are subdued and encompass longer intervals (Fig. 6). Chiggiato et al.

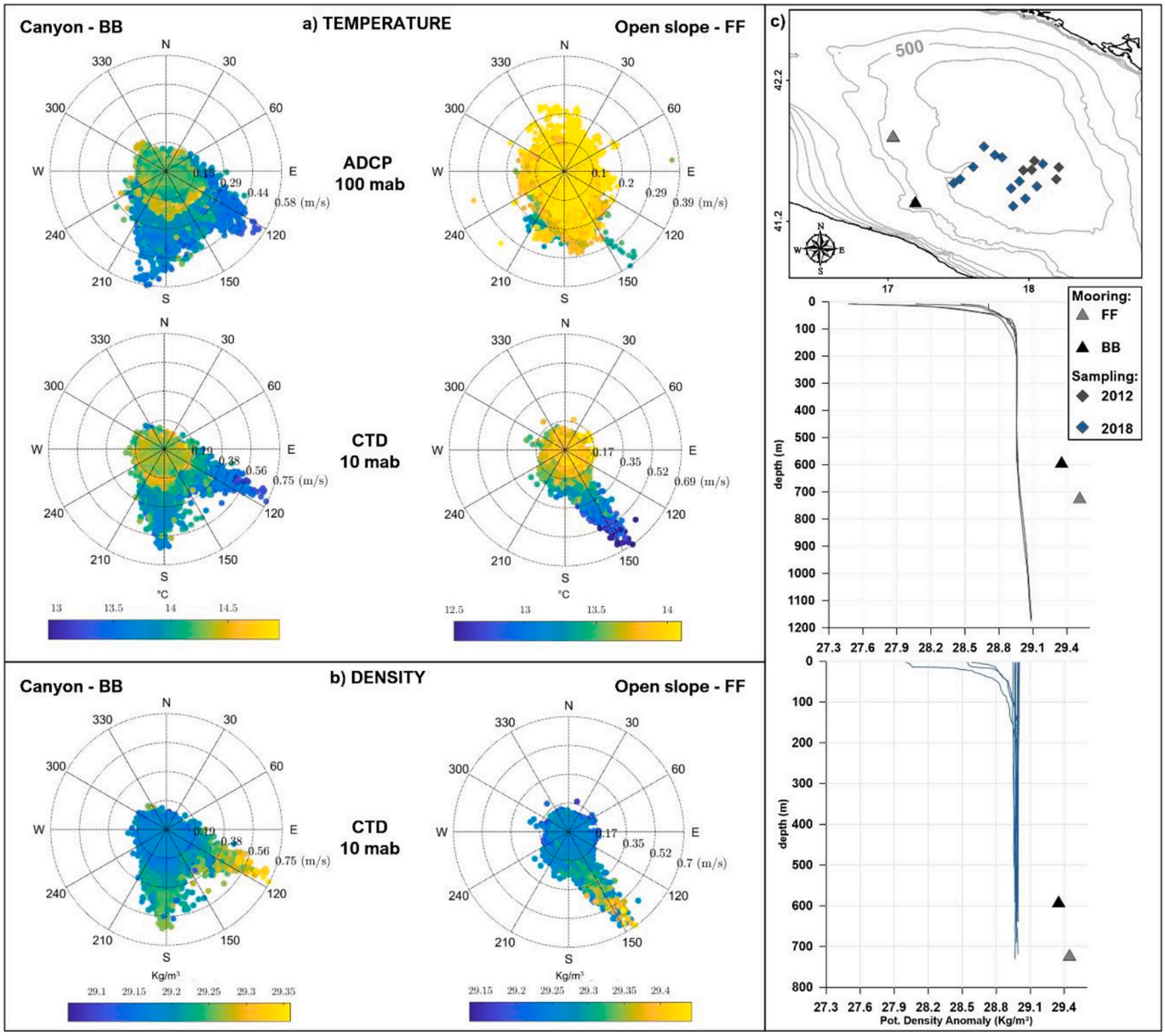

Fig. 5. Polar plot of currents in BB (canyon) and FF (open-slope) at two depths of the water column (10 and 100 mab). In panel (*a*) colours refers to T whereas in panel (*b*) to σ. Note that colour scales used for the two moorings are different; c) Argo float σ profiles recorded in 2012 and 2018 in the South Adriatic (The profile positions are represented in the map by squares) compared to maximum σ measured at the mooring in the same period (triangles). The data are retrieved from Coriolis database https://dataselection.coriolis.eu.org/.

Table 2
Number of days of cascading events that were selected from the yearly datasets of the two sites, to be considered for the analysis.

Year	Days	
	BB	FF
2012	11	31
2013	2	7
2017	3	42
2018	21	31
2019	8	0

(2016a) quantified the different frequencies of DW pulses in the two sites, for the 2012 event in a sub-inertial period of 1.6 days at FF and 3 to 4 days at site BB. In addition, Bonaldo et al. (2018) demonstrated that the dynamic observed in the FF site is associated with the propagation of trains of Continental Shelf Waves (CSW) that behave differently along the continental margin depending on the geometric constraints of sea-floor topography. The CSW are a particular kind of topographic waves (Rhines, 1970; Pedlosky, 1987) propagating along the continental margin and trapped thereby as an effect of the pronounced bathymetry (Buchwald and Adams, 1968; Schulz et al., 2012). In the BB site the bimodal direction of the current field, already recognized in previous measurements (Turchetto et al., 2007; Chiggiato et al., 2016a), is confirmed on the longer time-series presented here. DW cascading flow along the canyon-axis (south-east ward) while another cold-water mass propagates southward having reached its equilibrium level as a geo-strophycally adjusted flow (Chiggiato et al., 2016a). Although the characteristics of the cascading currents remain visible even when they reach the basin floor, the downward energetic plumes are very efficient in mixing with ambient waters, which results in a progressive thickening of the downward flow and an attenuation of the original thermohaline

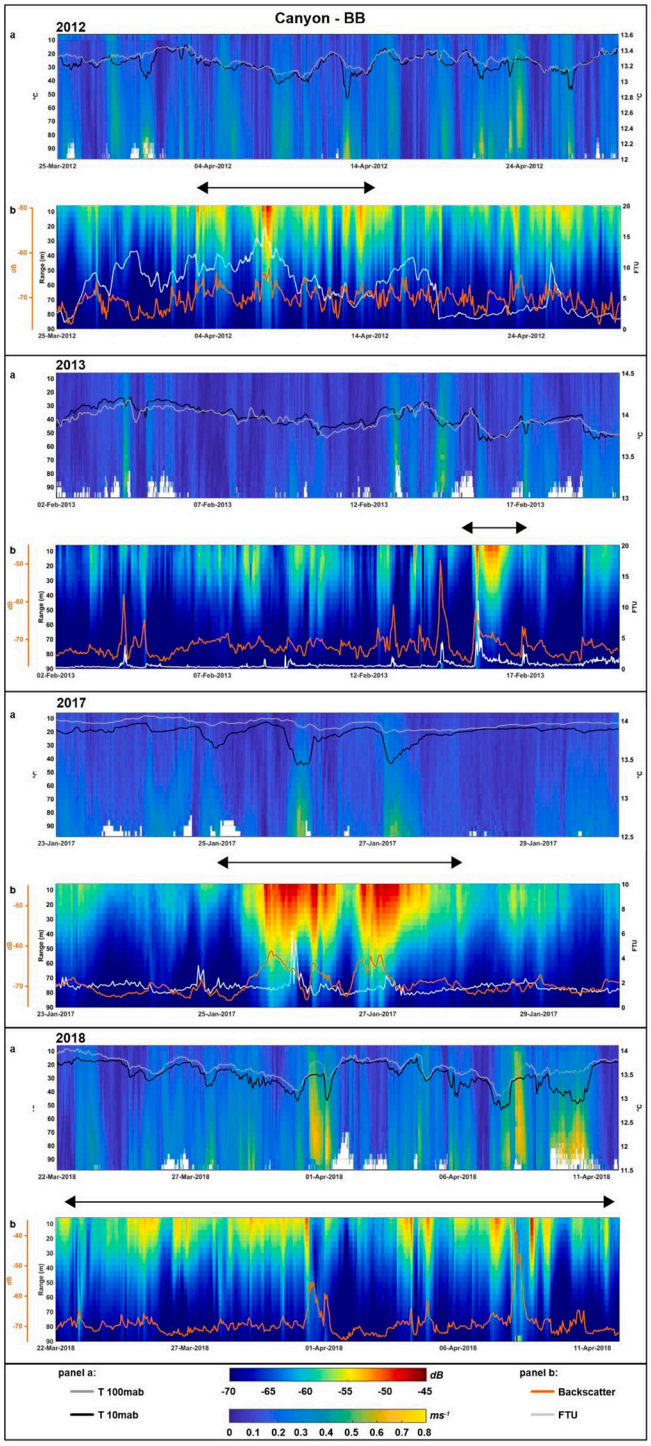

Fig. 6. Selected cascading events recorded in the mooring site BB (canyon). For each panel, (a) depicts the distribution of the current speed along space and time and the time-series of T measured at 10 mab (black line) and in correspondence of the ADCP (grey line) at 100 mab. In (b) the diagram represents the distribution of the backscatter signal along space and time; the white line is turbidity measured at 10mab and the orange line is the backscatter extracted from the corresponding cell of the turbidimeter. The double arrow indicates the time range of cascading events selected from the datasets shown in Table 2 and Fig. 9 for the mooring BB.

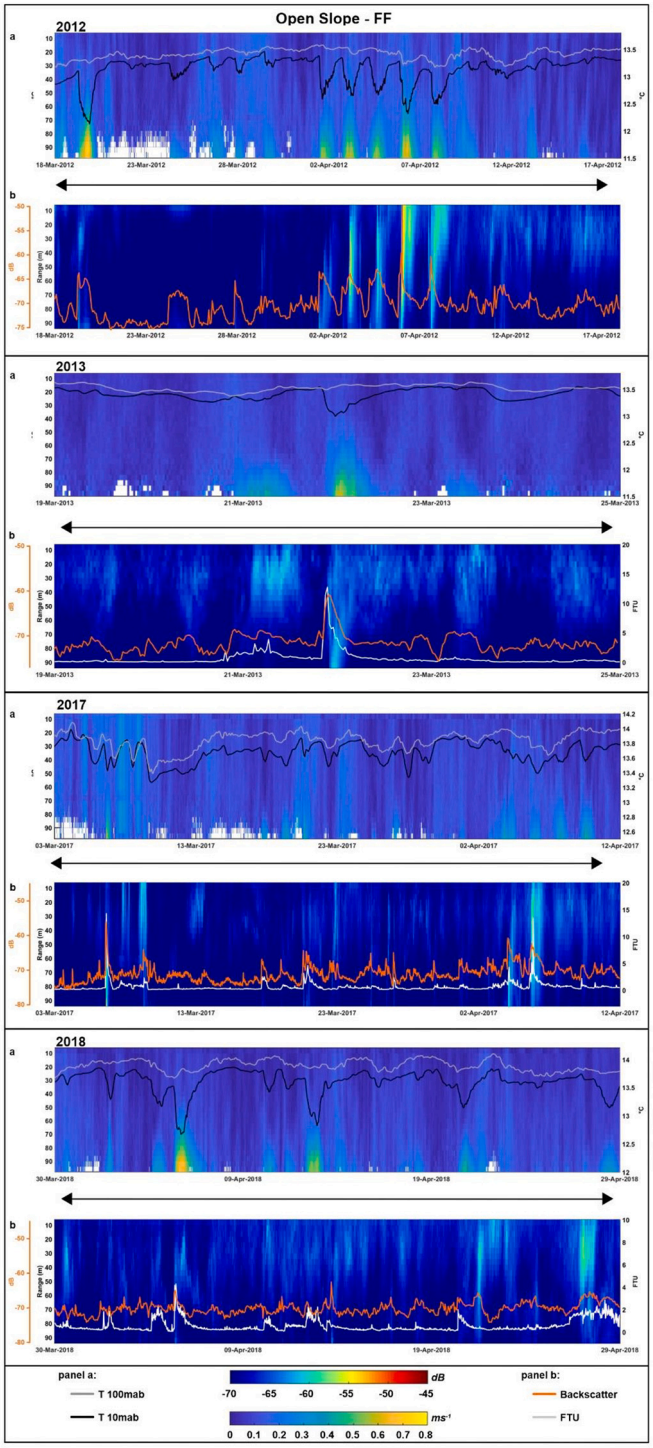

Fig. 7. Selected cascading events recorded in the mooring site FF (open slope). Keys as in Fig. 6. The double arrow indicates the time range of cascading events selected from the datasets shown in Table 2 and Fig. 10 for the mooring FF.

characteristics (Rubino et al., 2012; Chiggiato et al., 2016a). Although a mixing process is active during the sliding along the slope, the cascading currents have a higher σ (during the most intense events in 2012 and 2018 exceeded 0.27 Kgm^{-3}) than elsewhere along the slope at the same depth, demonstrating how their equilibrium level is much deeper that the depth of the mooring sites. Previous observations by Manca et al. (2003) indeed found a NAdDW layer below 800 m occupying the deepest part of SAP. These water masses sustained the outflow trough the Otranto strait, feeding the bottom waters of Eastern Mediterranean

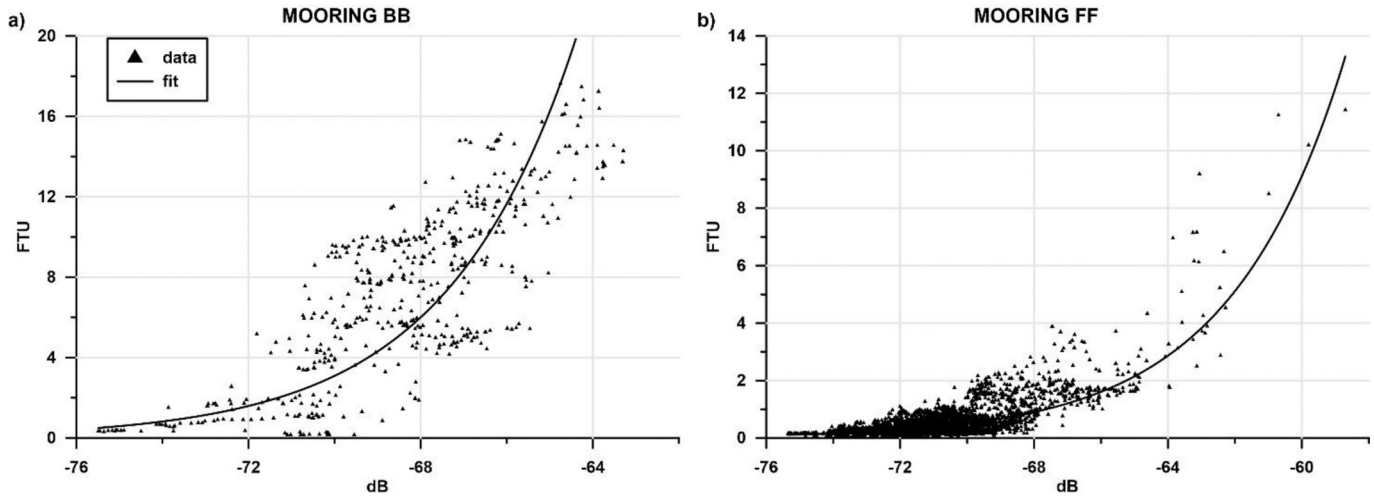

Fig. 8. Regression between backscatter (x-axis) and turbidity (y-axis) in the two mooring sites BB (canyon, a) and FF (open slope, b).

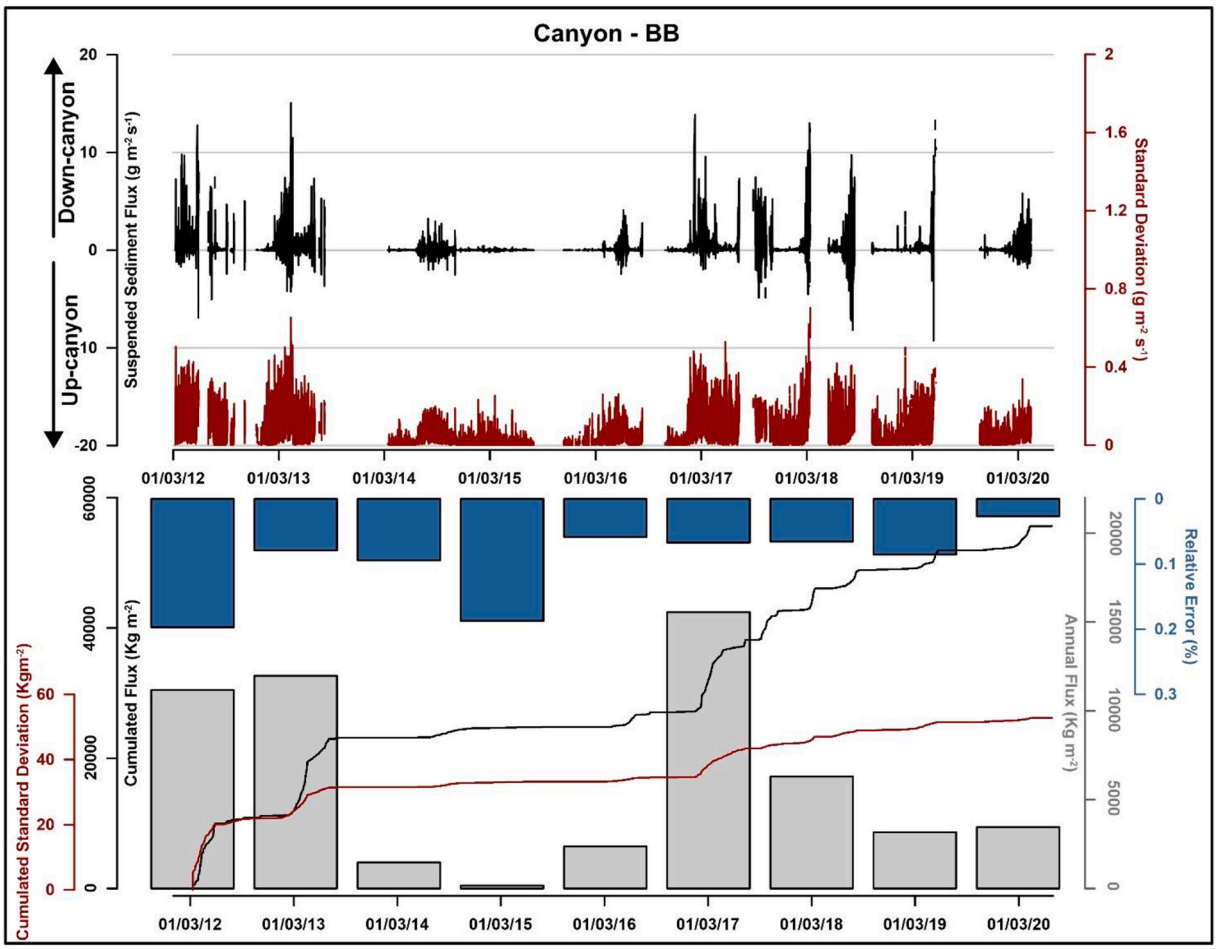

Fig. 9. a) Instantaneous SF across the section passing from the BB site (black line); red line indicates the standard deviation. b) Cumulated flux and standard deviation (black and red lines); bars indicate the annual flux (grey) and Relative Error (blue). (For interpretation of the references to colour in this figure legend, the reader is referred to the web version of this article.)

Sea.

5.2. Characteristics of near bottom sediment flux

The coupled analysis of turbidity and current data in section 3.6 allowed the definition of the instantaneous and cumulative near-bottom SFs across two sections of the continental slope, establishing the solid contribution per unit area, and of relative uncertainty of the estimates done. In both sites the sharp increases in the cumulative down-slope SF, represented in Figs. 9b and 10b, are linked to DW passage events and concentrated between February and May (Paladini de Mendoza et al., 2022a) The annual SF at the BB site exhibits an oscillation. The years of

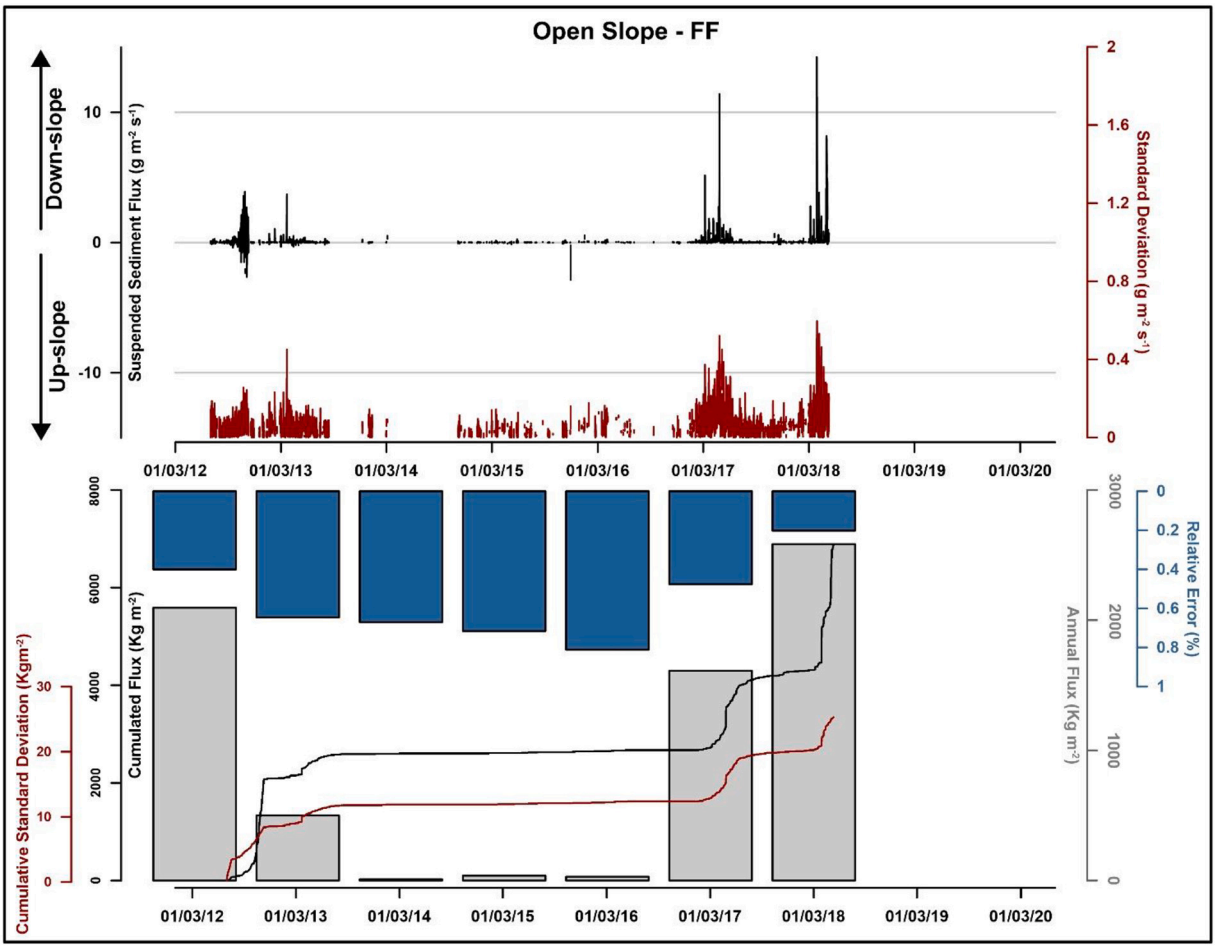

Fig. 10. Instantaneous, cumulate and annual SF across the section passing from the FF site and relative standard deviations and error. Keys as in Fig. 9.

maximum contribution to the total SF were 2012, 2013, 2017 and 2018 with evidences of DW cascading phenomena (Chiggiato et al., 2016b; Paladini de Mendoza et al., 2022a) while the years without cascading events, (between 2014 and 2016) have a negligible contribution to the total annual SF budget. The sum of the years characterised by cascading events represents 80% (BB) and 98% (FF) of the total solid contribution and the residual percentage suggests that the canyon is affected by particulate transport even in the absence of DW flows, while the open slope appears to be affected almost exclusively by these events. Comparing the two sites during the same interval, in BB a flux about 7 times higher than at FF is observed, confirming how the canyon is a preferential sediment transport route to the deep sea.

SF recorded along the slope in the two sites can be compared with those impacting two canyons (Duthiers Canyon and Cap de Creus Canyon) and in the open slope of the Gulf of Lion (Palanques et al., 2012) from October 2005 to October 2006 where IFs vary by >4 orders of magnitude, between 1×10–3 g m^{-2} s^{-1} at the deepest sites (1500 m) and >94 g m^{-2} s^{-1} at 300 m in Cap de Creus, where the greatest transport occurs. At the mooring located at 300 m depth at Cap de Creus, the cumulative SF during the year of measurement reaches about 8000 Kg m^{-2}, which decreases to 3000 at the deepest mooring (1000 m). In the open slope sector, transport along the slope amounts to about 2000 Kg m^{-2} at 1000 m depth and 300 Kg m^{-2} at 1900 m. Previous investigations of approximately 6-months from November 2003 to May 2004 at Cap de Creus (Palanques et al., 2006) show SFs between 150 and 3000 Kg m^{-2}, based on water column stratification conditions, storm intensity and fluvial input. In our study, the maximum IF recorded in the canyon and in the open slope between 2012 and 2020 are similar (respectively 18 g m^{-2} s^{-1} and 14 g m^{-2} s^{-1}), due to similar maximum velocity of recorded currents, but the annual total flux has a median of 500 Kg m^{-2} in the open slope (FF) and 3456 Kg m^{-2} in the canyon (BB). Quantifying in detail the contribution produced by the periods of largest transport, taking as reference the endpoints of the slope changes of the cumulative curve, we get values of 1274 and 2465 Kg m^{-2} for the years 2017 and 2018 in FF and 9711 and 8909 Kg m^{-2} in BB for the years 2012 and 2017, respectively, over a time interval ranging between 2 and 4 months. It is important to note that meteorological events that result in cascading events in the Gulf of Lion last only a few hours to 2–3 days, but cascading persists after the storm for about a week after the onset of the process (Palanques et al., 2006). The cascading events affecting the Adriatic margin although impulsive in character are much more prolonged in time. In fact, DW currents impact the continental margin over a 6-months window (generally from late January to early June) where the most energetic phase is concentrated between February and May (Paladini de Mendoza et al., 2022a).

5.3. Evaluation of sedimentary processes triggered by cascading events

The role of the DW masses on sediment and particulate transport in the deep-sea during cascading is recognized (Langone et al., 2016; Pellegrini et al., 2016; Trincardi et al., 2007b). The acceleration of flow during cascading implies that it exceeds a critical velocity threshold that can erode and resuspend seabed sediments, actively interacting with slope morphology (Bonaldo et al., 2016; Foglini et al., 2016; Pellegrini et al., 2016; Verdicchio et al., 2007; Trincardi et al., 2007a). Turbidity accompanying bottom currents below the critical velocity reflect transport of allochthonous particles, understood as particulate matter accumulated over time on the shelf and upper slope. Conversely, when

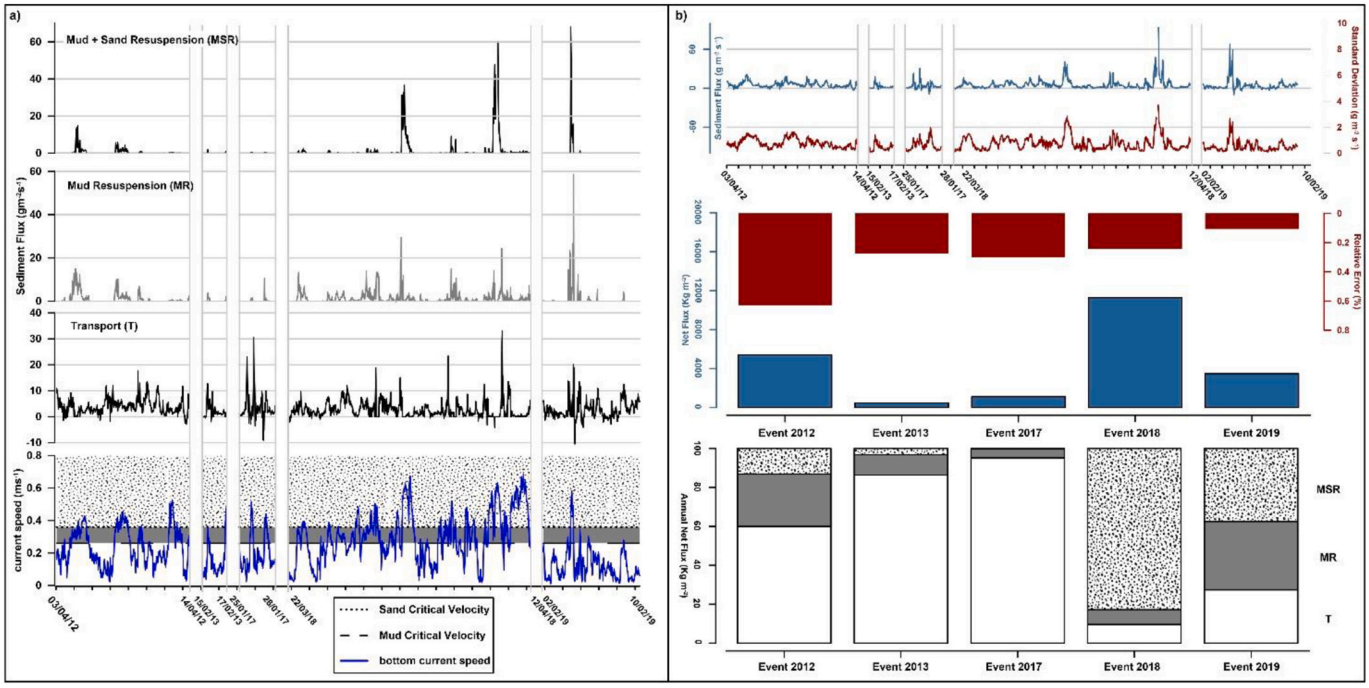

Fig. 11. (a) The SF during selected events in the canyon (BB) is divided in the different dynamic components depending on the velocity of the flow which is represented in the bottom graph. Moving downward there is the resuspended flux of mud and sand, the resuspended flux of mud and the transport component flux. The continuous line indicates the bottom current, the dashed line indicates the critical velocity for mud resuspension (0.26 ms^{-1}), the dash and dot line indicates the critical velocity threshold for sand resuspension (0.36 ms^{-1}). b) in the upper panel instantaneous SF (blue) and standard deviation (red) during selected events in the BB site (canyon), in the middle bars represents the net flux quantified for each event (blue) and their relative error (red); at the bottom the percentage of Mud and Sand Resuspension (MSR), Mud Resuspension (MR) and Transport (T). (For interpretation of the references to colour in this figure legend, the reader is referred to the web version of this article.)

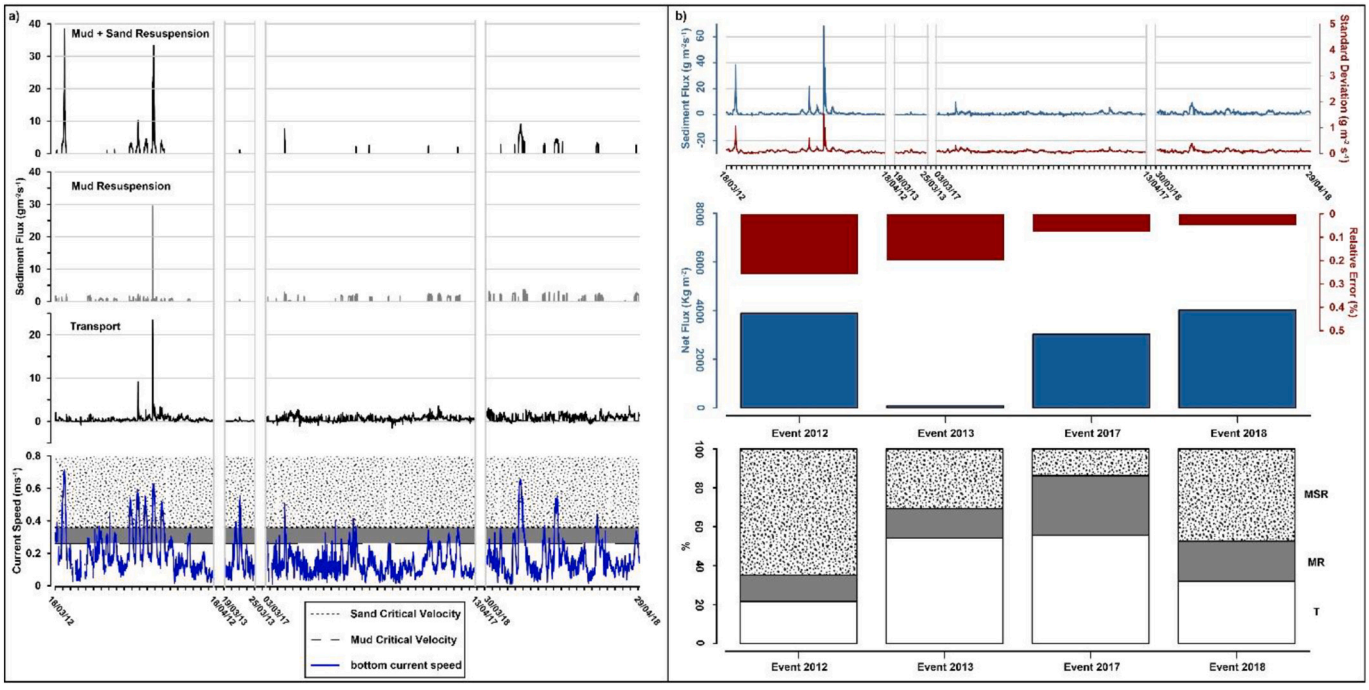

Fig. 12. (a) The SF during selected events in the canyon (FF), key as Fig. 11 b) in the upper panel IF and standard deviation during selected events in the FF site (canyon), in the middle the net flux quantified for each event and their relative error; at the bottom, the percentage of Mud and Sand Resuspension (MSR), Mud Resuspension (MR) and Transport (T), key as Fig. 11.

bottom currents exceed the critical velocity threshold, resuspension occurs adding particles to the flow as shown in Figs. 11 and 12 where IF is shown together with the velocity of bottom currents. Evidences about the resuspension processes and advection of allochthonous particles come from previous observations conducted in the BCS (Trincardi et al., 2007a) where the presence of foraminifera species *G. inflata*, generally

disappeared in Adriatic deposits related to the modern sea level high-stand (circa 6-kyr BP) (Jorissen et al., 1993; Asioli, 1996; Capotondi et al., 1999; Ariztegui et al., 2000), is ascribed to a component of re-sedimentation and deposition by either slope parallel currents or by sediment shedding from shallower waters.

The size of resuspended particles depends on the magnitude of current velocity (critical shear-stress) and the sediment grain-sizes on the impacted seabed. In BB, the bottom currents measured in 2018 were particularly intense and able of triggering extensive resuspension of seabed sediment in both of the grain-size representative of the seabed. During the other events, however, resuspension largely involved the mud component. The hydrodynamic field in FF during cascading is characterised by strong short-lived currents pulses (Chiggiato et al., 2016a) able to trigger the resuspension of the seabed sediments. Cascading currents were particularly strong during 2012 while they were less intense in the other years, especially in 2017, when the transport component was dominant, because currents rarely exceeded the threshold for the resuspension of fine sand grains (D = 0.2 mm). These considerations are not supported by samples that allow quantification of the different particle size fraction moved, but the distribution of the backscatter signal (with signal increases near the seafloor during current peaks) allows qualitative validation of resuspension processes that may have occurred during cascading events, the observation of which is extremely difficult given the depths of measurement and the characteristics of the events, which turn out to be sporadic and impulsive. Future investigations are to necessary address in detail the determination of the grain-size of the transported and resuspended particles.

Different acoustic frequencies are sensitive to different particle sizes. Sensitivity is defined as the volume scattering strength for a given concentration. Optical turbidity sensors that sample a small volume (approximately 1.10^{-6} m^3) are preferentially sensitive to fine particles. In fact, the measured optical turbidity for a given concentration of suspended particles increases as particle size decreases, due to both increased abundance and light scattering by smaller particles. For acoustic measurements, the ADCP used in this work, with a frequency of 307 kHz, has a peak sensitivity for particles of 0.12 mm in diameter (Lohrmann, 2001) and its sensitivity varies proportionally to the radius of the particles to the fourth power for smaller particles, while for larger particles the sensitivity is inversely proportional to particle radius. At station FF, backscatter signals are observed to be well defined at peak currents, and this concordance may be due to the dominance of bottom sediment resuspension processes in which the fine sand component is high. In contrast, the lower concordance in the canyon may be attributable to the high transport component and the greater heterogeneity of the grain-size populations.

Resuspension is a notable process, but with differences between sites, and the backscatter signal near the bottom during current pulses provides direct evidence of the active role played by currents in bottom reshaping. The bedform patterns observed by Trincardi et al. (2007a, b) and Foglini et al. (2016), in the canyon and surrounding open slope are the signatures attributed to DW passage, in agreement also with the results inferred from modelling experiments (Bonaldo et al., 2016). In BB, transport processes are very important and much of the resuspended material is fine-grained (Fig. 11b). In FF, resuspension has become the dominant process during selected events. The pulse of the currents at this site, which can reach high intensities in a short time, may be able to resuspend both size classes of sediment considered, producing the erosional traces inferred from the extensive presence of abyssal furrows oriented along the main direction of the currents (Verdicchio et al., 2007; Bonaldo et al., 2015). The SF obtained from turbidimeter records (section 4.3) and from backscatter (section 4.4) are compared considering the flux on a daily scale on the same time-interval of the observations. The SF estimated from the acoustic data has a value for site BB of 373±15 Kg m^{-2} d^{-1} compared with a value of 109±0.13 Kg m^{-2} d^{-1} obtained from turbidimeter. As for the FF site from the backscatter data, a SF of 89 +/− 0.16 Kg m^{-2} d^{-1} was obtained compared with 12 +/− 0.06 Kg m^{-2} d^{-1} obtained from the turbidimeter data. Obtained values have a reasonably agreements and differences can be traced to the ability on the part of the acoustic source to observe a larger water layer considering the vertical variability of the flux. At site BB, as previously mentioned, the DWs flow involving a water layer up to 80 m thick while in FF the active layer is never >40 m (Rubino et al., 2012; Chiggiato et al., 2016a; Paladini de Mendoza et al., 2022a). Results about the SF reported at daily scale on the basis of the number of days of selected events (Table 2) gives a value 5 time higher in BB than in FF. Our results highlight that the canyon is a preferred sediment transfer pathway, confirming previous results on its main role as an active conduit for sediment during high sea level conditions when it is far from the coast (Turchetto et al., 2007; Foglini et al., 2016; Langone et al., 2016). The SF for the unit of area for each site is extended to two 2-dimensional sections whose representativeness is determined along the vertical dimension by the variability observed from acoustic measurements and along the horizontal dimension by the morphological unit considered. For the canyon section (BB) the total solid load amounts to a value of 0.72 +/− 0.002 Tg, while in the open slope (FF) section it amounts to 1.17 +/− 0.0016 Tg for a total of 1.89 Tg of sediment transported across the 30-km long considered sections on the continental slope. The estimation done considers the vertical variation of flow at the mooring point and the geometry of the considered morphological unit but does not consider the real geometry of the dense tongue along the section. Relative to the canyon, the knowledge about the dense flow trajectory defines a preferential transit of the suspended sediment in the north branch (Trincardi et al., 2007a) but it has also been seen that from the hydrodynamic and thermohaline point of view the two branches have similar behaviour (Rubino et al., 2012, Chiggiato et al., 2016a). The south branch also has an edge that constrains the flow within it and the flow in the north branch in the lower part also passes to the south branch. Based on these considerations, the mooring measurements were considered representative of the whole canyon section, but an assessment of the actual geometry of dense flow within the canyon along the cross-sectional plane is lacking, and this dynamic aspect will need future investigation. Previous studies (Berntsen et al., 2016; Wåhlin, 2002) have observed that flow geometry within canyon is variable and determined primarily by topography and magnitude of bottom friction. Cross-sections within Cap de Creus canyon (Canals et al., 2006) showed that the dense flow has an asymmetric path and the turbid, dense tongue flows along the southern canyon wall.

Previous estimates conducted by Frignani et al. (2005), quantified the sediments exported from the northern and central Adriatic to the deep southern Adriatic basin and/or the Mediterranean Sea through the Strait of Otranto as 4.6 Tg $year^{-1}$. In addition, Lopes-Rocha et al. (2017) estimated ca. 3.0 Tg $year^{-1}$ of sediment accumulating on the Apulian continental shelf. Our estimates, which amount to 0.43 Tg $year^{-1}$ are obtained considering the most intense phase of cascading able to produce and clear backscatter signals and account for a maximum frequency of 42 days per year (Table 2). Also, the determination is limited to a relatively small portion of the continental margin (about 15%) of the approximately 200 km long shelf edge that is affected by the cascading DW following the results of numerical simulations by Rubino et al. (2012) and Bonaldo et al. (2018). On the other hand, the sediment load estimated by Frignani et al. (2005) and Lopes-Rocha et al. (2017) refers to reconstruction obtained from the total mass balance considering input and accumulation on sedimentary deposits of the western Adriatic continental shelf over a century time scale. Observations during the eight years of measurements show that these current pulsations represent the main hydrodynamic process (Paladini de Mendoza et al., 2022a) in which flow accelerations, directed down the slope, correspond to thermohaline changes that indicate the passage of DW (as seen in Fig. 5). What has been observed in this experiment, combined with the results of previous studies obtained with different methodologies (Turchetto et al., 2007; Langone et al., 2016; Foglini et al., 2016) confirms the main active role of cascading in the particulate transport to the

deep basin, but provides a more precise estimate of the dynamics of solid transport by defining the relative contributions on the mass balance of the two sectors of the slope characterised by different morphological and dynamic characteristics. In addition, it made it possible to assess the sedimentary processes that may occur during cascading by defining the contribution of resuspension induced by currents on the seabed.

Dense water cascading is a common process distributed worldwide (Ivanov et al., 2004) and concentrated especially from sub-tropics to high-latitude. In sub-tropics and mid-latitude area cascading events will be less frequent with climate warming (Ivanov and Watanabe, 2013: Durrieu de Madron et al., 2023) while at high-latitude cascading is favoured by ice-cover regression (Ivanov and Watanabe, 2013; Dong et al., 2017). In any case, sedimentary processes linked to these phenomena, support knowledge of the recognized important implications about the sedimentology and modern carbonate platform and off-shelf siliclastic environments (Wilson and Roberts, 1995) and particle dispersion pathways across the coastal margin (Durrieu de Madron et al., 2023) with a global significance.

Total sediment budget calculations on a basin scale are commonly carried out through estimates of accumulation rates reconstructed from sediment cores that are necessarily over long-time scales. In this study, we emphasise the role of constraining short-lived events and their products, both chronologically and in terms of sediment volumes. This approach can significantly improve the interpretation of the sedimentary records, where individual layers may be difficult to resolve. Indeed, recent study demonstrated the difficult to show from sediment cores the current impact of the input or erosion by dense water plunges on recent sedimentation (Durrieu de Madron et al., 2020).

6. Conclusions

The monitoring activities conducted along the western Adriatic margin have produced a long time series that provides an important observatory of deep-water dynamics. The study area is impacted by DW cascading events that are crucial in shelf-deep ocean exchange and deep seafloor re-shaping processes. In this work, we analyse SF recorded from 2012 and 2020 with a focus on processes triggered by the DW passage through a multiple approach including the use of an acoustic source with extremely high spatial and temporal resolution. Ancillary sedimentological data allowed us to separate the phases in which the dense currents may actively erode the seabed from those in which particles are transported within the dense flow. The average annual SF at the study sites is quantified with an uncertainty of 0.09% (BB) and 0.36% (FF) to 6181 Kg m^{-2} y^{-1} in the canyon and 981 Kg m^{-2} y^{-1} in the open slope with a contribute more than five time larger in the canyon, which is active and represents a preferential pathway of sediment transfer to deep basin. The analysis of fluxes across the continental margin has quantified the main role of canyons that represent the major geomorphic feature of continental margins around the world, enhancing knowledge about their ecological role in the transfer of matter and energy from the shelf to the deep sea that remains primary even in cases where it far from the coast. The years in which the greatest transport occurs are characterised by cascading events that collectively account for >80% of the total solid contribution, providing a primary role on the cross-shelf SF budget. The DW cascading events are characterised by annual and interannual fluctuations of their intensity, understood as the σ and velocity of cold currents, and their sediment transport capacity have a site-specific dynamic behaviour. The canyon is most affected by allochthonous particulate transport while on the open slope minor sediment transport occurs but particularly intense currents concentrated in a narrow layer near the bottom confer dynamic features that are mostly erosive. The sediment export from the shelf is concentrated during cascading current pulses but the DW transit along the SAM is more diluted in time respect others Mediterranean site. The genesis of DW cascading is linked to large atmospheric synoptic settings, and therefore climate change implicate shift on cascading rate opening possible scenarios for the evolution of cross-shelf dispersion pathways of particles, biogeochemical cycles and circulation dynamic with a global perspective. Continued monitoring is essential both for the analysis of long-term variations in the phenomena but also for implementing outstanding issues. Further investigations should be directed toward a quantitative assessment of resuspension processes that would allow linking the hydrodynamic regime and the size of the particles mobilized. This would also allow a more precise definition of uncertainties induced by different sensitivity of optical and acoustic instruments with respect to heterogeneous sedimentological population. In addition, more accurate determination of the geometry of the dense flow can improve the SF definition and its dynamic behaviour. By focusing on the accurate characterization of short-lived events, this study can provide critical support for the high-resolution interpretation of the stratigraphic records, and the large temporal extent of observation might serve as a reference for the quantification of Quaternary sediment budgets.

Declaration of Competing Interest

The authors declare that they have no known competing financial interests or personal relationships that could have appeared to influence the work reported in this paper.

Data availability

All data used in this study are made publicly available through the Zenodo repository. The registered database DOi for hydrodynamic (ADCP) and thermohaline data (CTD) is doi.org/10.5281/zenodo.6770202 (Paladini de Mendoza et al., 2022b). All information about surveys, maintenance operations, instrument calibrations, deployment configurations, data processing and quality control procedures during measurement period are detailed in the datapaper by Paladini de Mendoza et al., 2022a. Regarding echo intensity data from which backscatter is calculated and turbidity data the registered database DOi is doi.org/10.5281/zenodo.7586134 (Paladini de Mendoza et al., 2023).

Acknowledgements

The authors are first of all grateful to the reviewers for their comments, thanks to which a significant improvement of the work was achieved. This research was supported by the Italian Ministry of University and Research under the PRIN 2017 program project number 2017ASZAKJ "The Po-Adriatic Source-to-Sink system (PASS): from modern sedimentary processes to millennial-scale stratigraphic architecture". The maintenance of BB and FF fixed moorings over time was only possible thanks to the support of the following projects: European Community's Seventh Framework Programme projects HERMIONE (Grant agreement No. 226354) and COCONET (Grant agreement No.287844) of the European Commission, the Flagship project RITMARE SP5_WP3_AZ1 (the Italian Research for the Sea). This work was supported also by the EMSO-Italia Joint Research Unit (JRU). The authors thank the cruise participants who helped with the mooring servicing, in particular the captain and the crew members of the R/V's Urania, Minerva Uno, G. Dallaporta, Laura Bassi and OGS Explora, and of the fishing boats Pasquale & Cristina, and Attila.

Appendix A. Appendix

The bottom shear stress may be taken as an expression for the drag force, the mobilizing force, acting on individual sediment grains on the bed surface. The shear stress (Nm^{-2}) is obtained by the equation

$$\tau_c = \rho U^{*2} \tag{1}$$

Where U^* is the current shear velocity (ms^{-1}) and ρ is the density of water (kgm^{-3}).

The shear velocity is derived by the equation:

$$U^* = \sqrt{(f_c/2)}U \tag{2}$$

Where f_c is the current friction factor and U is the current velocity at the bottom (ms^{-1}),

The critical shear velocity for each sediment class is obtained by the equation proposed by Madsen and Wood (2002):

$$U_{*cr} = \sqrt{(s-1)gD}\sqrt{\phi cr} \tag{3}$$

Where ϕcr is the critical value of the Shields parameter, s is the ratio between sediment and water density, and D is the grain size (D_{50}, mm). The critical shear stress is derived from the critical shear velocity in the same way of (1). The Shields curve defines a unique relationship between ϕcr and Re*.

The ϕcr is directly derived from the sediment-fluid parameter (S_*) as described in Madsen and Grant (1976).

$$S_* = \frac{D}{4\nu}\sqrt{(s-1)gD} = \frac{Re^*}{4\sqrt{\phi cr}} \tag{4}$$

Where ν is kinematic viscosity of the fluid (m^2s^{-1}) and g is the gravity (ms^{-2}).

If $S_* < 0.8; \phi cr = 0.1 S_*^{-2/7}$;

If $0.8 < S_* < 300$; ϕcr is determined graphically from the "Modified Shields diagram" (Madsen and Grant, 1976);

If $S_* > 300; \phi cr \approx 0.06$.

Appendix B. Appendix

The Backscatter (BS) is determined by the Mullison (2017) formulation

$$BS = C + 10log\,(T_x + 237.16)\,R^2 - L_{bdm} - P_{dbw} + 2\alpha R + 10log((k_c(E - E_r)/10\,) - 1\,) \tag{5}$$

The term E (measured in counts) is the Returned Signal Strength Indicator (RSSI) amplitude, reported by the ADCP for each bin along each beam; E_r is the reference noise floor RSSI amplitude. The k_c is a conversion factor of the amplitude counts reported by the ADCP's receive circuitry to decibels (dB). The parameter E_r is constant for each beam of a given ADCP and is available from factory parameters calibration. In the computation we applied all E_r and k_c coefficients provided by RDI for every acoustic beam of every ADCP used. The terms of eq. (5) that depends on the ADCP system used and sampling plan are summarised in Table 3.

C is an instrumental constant of RDI profilers of the typer Workhorse Sentinel Broadband ADCP 307 kHz. L_{dbm} is the $10\log_{10}$(transmit pulse length, L) and P_{dbw} is the $10\log_{10}$(transmit power, W) defined by RDI for the ADCP model used. T_x is real-time temperature of the transducer, R is the slant range, which is the range to the relevant scattering layer along the beam and is calculated by:

$$R = [(B + (L + D)/2 + (N-1)\,D + (D/4)\,)/cos\theta]\,c^{'}/c1 \tag{6}$$

where B is blank after transmit, D the depth cell length, N the depth cell number of the scattering layer being measured, θ is the beam angle, c' is the average sound speed from the transducer to the range cell and c1 is the speed of sound used by the instrument.

The transmission lost along the water column depends on absorption of acoustic energy by the sea water. The absorption for each range cell, $\alpha n = 2\alpha D/\cos(\theta)$ where α is the absorption coefficient at that depth. The value of 2αR is determined by:

$$2\alpha R = (2\alpha\beta/cos\,\theta) + \sum_{n-1}^{b}\alpha^{'n} \tag{7}$$

Where α' is the absorption at the profiler and b is the range cell number.

The absorption coefficient is calculated by the algorithms of Bill Stevens (2022) which used the Fisher and Simmons (1977) and Ainslie and McColm (1998) equations based on viscous absorption generated by particle motion and absorption by specific chemicals reported in Kinsler et al. (2000).

The oceanographic parameters of salinity and temperature used for the determination of the coefficient α are retrieved by the measurements conducted on the mooring by the SBE probe

Table 3
Parameters of Eq. (5).

Term	Value
C	−143.5
L (m)	4.36
D (m)	4

(*continued on next page*)

Table 3 (*continued*)

Term	Value
B (m)	6.19
W (dBW)	14
Θ (°)	20

References

Ainslie, M.A., McColm, J.G., 1998. A simplified formula for viscous and chemical absorption in sea water. J. Acoust. Soc. Am. 103 (3), 1671–1672. https://doi.org/10.1121/1.421258.

Allen, S.E., Durrieu de Madron, X., 2009. A review of the role of submarine canyons in deep-ocean exchange with the shelf. Ocean Sci. 5, 607–650. https://doi.org/10.5194/os-5-607-2009.

Ariztegui, D., Asioli, A., Lowe, J.J., Trincardi, F., Vigliotti, L., Tamburini, F., Chondrogianni, C., Accorsi, C.A., Bandini Mazzanti, M., Mercuri, A.M., van der Kaars, S., McKenzie, J.A., Oldfield, F., 2000. Palaeoclimate and the formation of sapropel S1: inferences from late Quaternary lacustrine and marine sequences in the Central Mediterranean region. Palaeogeogr. Palaeoclimatol. Palaeoecol. 158, 215–240. https://doi.org/10.1016/S0031-0182(00)00051-1.

Asioli, A., 1996. High-resolution foraminifera biostratigraphy in the central Adriatic basin during the last deglaciation: a contribution to the Paliclas Project. In: Guilizzoni, P., Oldfield, F.L. (Eds.), Palaeoenvironmental Analysis of Italian Crater Lake and Adriatic Sediments (PALICLAS project), 55. Mem. Istit. It. Idrob, pp. 197–217.

Berntsen, J., Darelius, E., Avlesen, H., 2016. Gravity currents down canyons: effects of rotation. Ocean Dyn. 66, 1353–1378. https://doi.org/10.1007/s10236-016-0981-8.

Bonaldo, D., Benetazzo, A., Bergamasco, A., Campiani, E., Foglini, F., Sclavo, M., Trincardi, F., Carniel, S., 2016. Interactions among Adriatic continental margin morphology, deep circulation and bedform patterns. Mar. Geol. 375, 82–98. https://doi.org/10.1016/j.margeo.2015.09.012.

Bonaldo, D., Orlic, M., Carniel, S., 2018. Framing Continental Shelf Waves in the southern Adriatic Sea, a further flushing factor beyond dense water cascading. Sci. Report. 8, 660. https://doi.org/10.1038/s41598-017-18853-2.

Buchwald, V.T., Adams, J.K., 1968. The propagation of continental shelf waves. Proc. Roy. Soc. A 305, 235–250. https://doi.org/10.1098/rspa.1968.0115.

Canals, M., Puig, P., Durrieu de Madron, X., Heussner, S., Palanques, A., Fabres, J., 2006. Flushing submarine canyons. Nature 444, 354–357. https://doi.org/10.1038/nature05271.

Capotondi, L., Borsetti, A.M., Morigi, C., 1999. Foraminiferal ecozone, a high resolution proxy for the late Quaternary biochronology in the Central Mediterranean Sea. Mar. Geol. 153, 253–274. https://doi.org/10.1016/S0025-3227(98)00079-6.

Chiggiato, J., Bergamasco, A., Borghini, M., Falcieri, F.M., Falco, P., Langone, L., Miserocchi, S., Russo, A., Schroeder, K., 2016a. Dense-water bottom currents in the Southern Adriatic Sea in spring 2012. Mar. Geol. 375, 134–145. https://doi.org/10.1016/j.margeo.2015.09.005.

Chiggiato, J., Schroeder, K., Trincardi, F., 2016b. Cascading dense shelf-water during the extremely cold winter of 2012 in the Adriatic, Mediterranean Sea: Formation, flow, and seafloor impact. Mar. Geol. 375, 1–4. https://doi.org/10.1016/j.margeo.2016.03.002.

Deines, K., 1999. Backscatter Estimation using Broadband Acoustic Doppler Current Profilers. In: Proc. Sixth Working Conf. On Current Measurement. IEEE, San Diego, CA, pp. 249–253.

Dong, L., Liu, Y., Shi, X., Polyak, L., Huang, Y., Fang, X., Liu, J., Zou, J., Wang, K., Sun, F., Wang, X., 2017. Sedimentary record from the Canada Basin, Arctic Ocean: implications for late to middle Pleistocene glacial history. Clim. Past 13, 511–531. https://doi.org/10.5194/cp-13-511-2017.

Durrieu de Madron, X., 2019. Propagation of uncertainty on parameters derived from time series. In: "Time Series Analysis" Conference and Training School in Tromsø. January 28, 2019 - January 31, 2019.

Durrieu de Madron, X., Aubert, D., Charrière, B., Kunesch, S., Menniti, C., Radakovitch, O., Sola, J., 2023. Impact of Dense Water Formation on the Transfer of Particles and Trace Metals from the Coast to the Deep in the Northwestern Mediterranean. Water 15 (2), 301. https://doi.org/10.3390/w15020301.

Durrieu de Madron, X., Stabholz, M., Heimbürger-Boavida, L.E., Voutquenne-Nazabadioko, L., Kerhervé, P., Wolfgang, L., 2020. Approaches to evaluate spatial and temporal variability of deep marine sediment characteristics under the impact of dense water formation events. Mediterr. Mar. Sci. 21 (3), 527–544. https://doi.org/10.12681/mms.22581.

Fisher, F.H., Simmons, V.P., 1977. Sound Absorption in Sea Water. J. Acoust. Soc. Am. 62 (3), 558–565. https://doi.org/10.1121/1.381574.

Flood, R.D., 1983. Classification of sedimentary furrows and a model for furrow initiation and evolution. Geol. Soc. Am. Bull. 94 (5), 630–639.

Foglini, F., Campiani, E., Trincardi, F., 2016. The reshaping of the South West Adriatic margin by cascading of dense shelf waters. Mar. Geol. 375, 64–81. https://doi.org/10.1016/j.margeo.2015.08.011.

Frignani, M., Langone, L., Ravaioli, M., Sorgente, F., Alvisi, F., Albertazzi, S., 2005. Fine-sediment mass balance in the western Adriatic continental shelf over a century time scale. Mar. Geol. 222–223, 113–133. https://doi.org/10.1016/j.margeo.2005.06.016.

Gartner, J.W., 2004. Estimating suspended solids concentrations from Backscatter intensity measured by Acoustic Doppler current profiler in San Francisco Bay, California. Mar. Geol. 211, 169–187. https://doi.org/10.1016/j.margeo.2004.07.001.

Gentil, M., Many, G., Durrieu de Madron, X., Cauchy, P., Pairaud, I., Testor, P., Verney, R., Bourrin, F., 2020. Glider-based active Acoustic monitoring of Currents and Turbidity in the Coastal Zone. Remote Sens. 12, 2875. https://doi.org/10.3390/rs12182875.

Glenn, S., Jones, C., Twardowski, M., Bowers, L., Kerfoot, J., Kohut, J.T., Webb, D., Schofield, O.M., 2008. Glider observations of sediment resuspension in a Middle Atlantic Bight fall transition storm. Limnol. Oceanogr. 53, 2180–2196. https://doi.org/10.4319/lo.2008.53.5_part_2.2180.

Guerra, D., Schroeder, K., Borghini, M., Camatti, M., Pansera, E., Schroeder, A., Sparnocchia, S., Chiggiato, J., 2019. Zooplankton diel vertical migration in the Corsica Channel (North-Western Mediterranean Sea) detected by a moored acoustic Doppler current profiler. Ocean Sci. 15, 631–649. https://doi.org/10.5194/os-15-631-2019.

Guillen, J., Palanques, J., Puig, P., Durrieu de Madron, X., Nyffeler, F., 2000. Field Calibration of Optical Sensors for Measuring Suspended Sediment Concentration in the Western Mediterranean. Scientia Marina 64, 427–435. https://doi.org/10.3989/scimar.2000.64n4427.

Harris, C.K., Butman, B., Traykovski, P., 2003. Winter-time circulation and sediment transport in the Hudson Shelf Valley. Cont. Shelf Res. 23, 801–820. https://doi.org/10.1016/S0278-4343(03)00025-6.

Holdaway, G.P., Thorne, P.D., Flatt, D., Jones, S.E., Prandle, D., 1999. Comparison between ADCP and transmissometer measurements of suspended sediment concentration. Cont. Shelf Res. 19, 421–441. https://doi.org/10.1016/S0278-4343(98)00097-1.

Ivanov, V.V., Watanabe, E., 2013. Does Arctic Sea ice reduction foster shelf–basin exchange? Ecol. Appl. 23 (8), 1765–1777. https://doi.org/10.1890/11-1069.1.

Ivanov, V.V., Shapiro, G.I., Huthnance, J.M., Aleynik, D.L., Golovin, P.N., 2004. Cascades of dense water around the world ocean. Prog. Oceanogr. 60 (1), 47–98. https://doi.org/10.1016/j.pocean.2003.12.002.

Jiang, L., Garwood, R.W., 1996. Three-dimensional simulations of overflows on continental slopes. J. Phys. Oceanogr. 26, 1214–1223. https://doi.org/10.1175/1520-0485(2004)034<2006:TTBDCF>2.0.CO;2.

Jorissen, F.J., Asioli, A., Borsetti, A.M., Capotondi, L., de Visser, J.P., Hilgen, F.J., Rohling, E.J., van der Borg, K., Vergnaud-Grazzini, C., Zachariasse, W.J., 1993. Late Quaternary Central Mediterranean biochronology. Mar. Micropaleontol. 21, 169–189. https://doi.org/10.1016/0377-8398(93)90014-O.

Kinsler, L.E., Frey, A.R., Coppens, A.B., Sanders, J.V., 2000. Fundamentals of Acoustics, Fourth ed. Wiley, New York. ISBN: 978–0–471-84789-2.

Langone, L., 2011. Obama_2011 Cruise Report, R/V Urania, Ravenna March 24 - Ancona, April 06, 2011.

Langone, L., Conese, I., Miserocchi, S., Boldrin, A., Bonaldo, D., Carniel, S., Chiggiato, J., Turchetto, M., Borghini, M., Tesi, T., 2016. Dynamics of particles along the western margin of the Southern Adriatic: processes involved in transferring particulate matter to the deep basin. Mar. Geol. 375, 28–43. https://doi.org/10.1016/j.margeo.2015.09.004.

Liu, J.T., Liu, J.K., Huang, J.S., 2002. The influence of a submarine canyon on river sediment dispersal and inner shelf sediment movements: a perspective from grain size distribution. Mar. Geol. 181 (4), 357–386.

Lohrmann, A., 2001. Monitoring sediment concentration with acoustic backscattering instruments. Nortek Tech. Note 3, 1–5.

Longdill, P.C., Healy, T.R., 2007. Sediment dynamics surrounding a flood tidal delta adjacent to reclamation and a dredge turning basin. J. Coast. Res. 23 (5), 1097–1105. https://doi.org/10.2112/04-0410.1.

Lopes-Rocha, M., Langone, L., Miserocchi, S., Giordano, P., Guerra, R., 2017. Spatial patterns and temporal trends of trace metal mass budgets in the western Adriatic sediments (Mediterranean Sea). Sci. Total Environ. 599-600, 1022–1033. https://doi.org/10.1016/j.scitotenv.2017.04.114.

Luneva, M.V., Ivanov, V.V., Tuzov, F., Aksenov, Y., Harle, J.D., Kelly, S., Holt, J.T., 2020. Hotspots of densewater cascading in the Arctic Ocean:Implications for the Pacific waterpathways. J. Geophys. Res. Oceans. 125 https://doi.org/10.1029/2020JC016044.

Lynch, J.F., Irish, J.D., Sherwood, C.R., Agrawal, Y.C., 1994. Determining suspended sediment particle size information from acoustical and optical backscatter measurements. Cont. Shelf Res. 14, 1139–1165. https://doi.org/10.1016/0278-4343(94)90032-9.

Madsen, O., Grant, W., 1976. Sediment Transport in the Coastal Environment. Tech. Rep. 209. M.I.T, Cambridge, Massachusetts, USA. https://hdl.handle.net/1721.1/142976.

Madsen, O.S., Wood, W., 2002. Sediment transport outside the Surf Zone. In: Vincent, L., Demirbilek, Z. (Eds.), Coastal Engineering Manual. U.S. Army Corps of Engineers, Washington, DC, p. 72.

Mahjabin, T., Pattiaratchi, C., Hetzel, Y., 2020. Occurrence and seasonal variability of Dense Shelf Water Cascades along Australian continental shelves. Sci. Rep. 10, 9732. https://doi.org/10.1038/s41598-020-66711-5.

Manca, B.B., Budillon, G., Scarazzato, P., Ursella, L., 2003. Evolution of dynamics in the eastern Mediterranean affecting water mass structures and properties in the Ionian and Adriatic Seas (1995e1999). J. Geophys. Res. Oceans 108, C9. https://doi.org/10.1029/2002JC001664.

Marini, M., Maselli, V., Campanelli, A., Foglini, F., Grilli, F., 2016. Role of the Mid-Adriatic deep in dense water interception and modification. Mar. Geol. 375, 5–14. https://doi.org/10.1016/j.margeo.2015.08.015.

Martín, J., Palanques, A., Puig, P., 2006. Composition and Variability of Downward Particulate Matter Fluxes in the Palamós Submarine Canyon (NW Mediterranean). J. Mar. Res. 60, 75–97. https://doi.org/10.1016/j.jmarsys.2005.09.010.

Mihanović, H., Vilibić, I., Carniel, S., Tudor, M., Russo, A., Bergamasco, A., Bubić, N., Ljubešić, Z., Viličić, D., Boldrin, A., Malačič, V., Celio, M., Comici, C., Raicich, F., 2013. Exceptional dense water formation on the Adriatic shelf in the winter of 2012. Ocean Sci. 9, 561–572. https://doi.org/10.5194/os-9-561-2013.

Mullison, J., 2017. Backscatter Estimation using Broadband Acoustic Doppler Current Profilers – Updated. In: Application Note, FSA-031. Instruments, Teledyne RD.

Murphy, P.L., Valle-Levinson, A., 2008. Tidal and residual circulation in the St. Andrew Bay system, Florida. Cont. Shelf Res. 28 (11), 2678–2688. https://doi.org/10.1016/j.csr.2008.09.003.

Paladini de Mendoza, F., Schroeder, K., Langone, L., Chiggiato, J., Borghini, M., Giordano, P., Miserocchi, S.. Moored echo and turbidity measurements in the Southern Adriatic Sea at mooring site BB and FF. Zenodo. https://doi.org/10.5281/zenodo.7586134.

Paladini de Mendoza, F., Schroeder, K., Langone, L., Chiggiato, J., Borghini, M., Giordano, P., Verazzo, G., Miserocchi, S., 2022a. Deep-water hydrodynamic observations of two moorings sites on the continental slope of the southern Adriatic Sea (Mediterranean Sea). Earth Syst. Sci. Data 14, 5617–5635. https://doi.org/10.5194/essd-14-5617-2022.

Paladini de Mendoza, F., Schroeder, K., Langone, L., Chiggiato, J., Borghini, M., Giordano, P., Verazzo, G., Miserocchi, S., 2022b. Moored current and temperature measurements in the Southern Adriatic Sea at mooring site BB and FF, March 2012-June 2020 (1.1) [Data set]. Zenodo. https://doi.org/10.5281/zenodo.7311090.

Palanques, A., El Khatab, M., Puig, P., Masqué, P., Sánchez-Cabeza, J.A., Isla, E., 2005a. Downward particle fluxes in the Guadiaro submarine canyon depositional system (north-western Alboran Sea), a river flood dominated system. Mar. Geol. 220 (1–4), 23–40. https://doi.org/10.1016/j.margeo.2005.07.004.

Palanques, A., Garcia-Ladona, E., Gomis, D., Martín, J., Marcos, M., Pascual, A., Puig, P., Emelianov, M., Guillén, J., Gili, J.M., Tintoré, J., Jordi, A., Basterretxeab, G., Font, J., Segura, M., Blasco, D., Monserrat, S., Ruiz, S., Pagès, F., 2005b. General patterns of circulation, sediment fluxes and ecology of the Palamós (La Fonera) submarine canyon, North-Western Mediterranean. Prog. Oceanogr. 66, 89–119. https://doi.org/10.1016/j.pocean.2004.07.016.

Palanques, A., Durrieu de Madron, X., Puig, P., Fabres, J., Guillén, J., Calafat, A., Canals, M., Heussner, S., Bonnin, J., 2006. Suspended sediment fluxes and transport processes in the Gulf of Lions submarine canyons. The role of storms and dense water cascading. Mar. Geol. 234 (1–4), 43–61. https://doi.org/10.1016/j.margeo.2006.09.002.

Palanques, A., Puig, P., Durrieu de Madron, X., Sanchez-Vidal, A., Pasqual, C., Martín, J., Calafat, A., Heussner, S., Canals, M., 2012. Sediment transport to the deep canyons and open-slope of the western Gulf of Lions during the 2006 intense cascading and open-sea convection period. Prog. Oceanogr. 106, 1–15. https://doi.org/10.1016/j.pocean.2012.05.002.

Pedlosky, J., 1987. Geophysical Fluid Dynamics. Springer-Verlag, New York.

Pellegrini, C., Maselli, V., Trincardi, F., 2016. Pliocene–Quaternary contourite depositional system along the south-western Adriatic margin: changes in sedimentary stacking pattern and associated bottom currents. Geo-Mar Lett. 36, 67–79. https://doi.org/10.1007/s00367-015-0424-4.

Pinardi, N., Estournel, C., Cessi, P., Escudier, R., Lyubartsev, V., 2022. Dense and deep water formation processes and Mediterranean overturning circulation. In: Schroeder, K., Chiggiato, J. (Eds.), Oceanography of the Mediterranean Sea, An Introductory Guide. Elsevier Inc., Amsterdam, pp. 209–252. ISBN: 978-0-12-823692-5.

Puig, P., Ogston, A.S., Mullenbach, B.L., Nittrouer, C.A., Sternberg, R.W., 2003. Shelf-to-canyon sediment-transport processes on the Eel continental margin (northern California). Mar. Geol. 193, 129–149. https://doi.org/10.1016/S0025-3227(02)00641-2.

Reichel, G., Nachtnebel, H.P., 1994. Suspended sediment monitoring in a fluvial environment: advantages and limitations applying an acoustic Doppler current profiler. Water Res. 28 (4), 751–761. https://doi.org/10.1016/0043-1354(94)90083-3.

Rhines, P., 1970. Edge, bottom, and Rossby waves in a rotating stratifed fuid. Geophys. Fluid Dyn. 1, 273–302. https://doi.org/10.1080/03091270093657769.

Ridente, D., Foglini, F., Minisini, D., Trincardi, F., Verdicchio, G., 2007. Shelf-edge erosion, sediment failure and inception of Bari Canyon on the Southwestern Adriatic margin (Central Mediterranean). Mar. Geol. 246 (2–4), 93–207. https://doi.org/10.1016/j.margeo.2007.01.014.

Rovere, M., Pellegrini, C., Chiggiato, J., Campiani, E., Trincardi, F., 2019. Impact of dense bottom water on a continental shelf: an example from the SW Adriatic margin. Mar. Geol. 408, 123–143. https://doi.org/10.1016/j.margeo.2018.12.002.

Rubino, A., Romanenkov, D., Zanchettin, D., Cardin, V., Hainbucher, D., Bensi, M., Boldrin, A., Langone, L., Miserocchi, S., Turchetto, M., 2012. On the descent of dense water on a complex canyon system in the southern Adriatic basin. Cont. Shelf Res. 44, 20–29. https://doi.org/10.1016/j.csr.2010.11.009.

Schieber, J., Southard, J.B., Schimmelmann, 2010. Lenticular shale fabrics resulting from intermittent erosion of water-rich muds—interpreting the rock record in the light of recent flume experiments. J. Sediment. Res. 80 (1), 119–128. https://doi.org/10.2110/jsr.2010.005.

Schulz, W.J., Mied, R.P., Snow, 2012. Continental shelf wave propagation in the Mid-Atlantic Bight: a general dispersion relation. J. Phys. Oceanogr. 42, 558–568. https://doi.org/10.1175/JPO-D-11-098.1.

Shi, J.Z., Zhang, S.Y., Hamilton, L.J., 2006. Bottom fine sediment boundary layer and transport processes at the mouth of the Changjiang Estuary, China. J. Hydrol. 327 (1–2), 276–288. https://doi.org/10.1016/j.jhydrol.2005.11.039.

Stevens, Bill, . Acoustic Absorption in Seawater. https://www.mathworks.com/matlabcentral/fileexchange/28653-acoustic-absorption-in-seawater. MATLAB Central File Exchange.

Thevenot, M.M., Prickett, T.L., Kraus, N.C., 1992. Tylers Beach, Virginia, Dredged Material Plume Monitoring Project 27 September to 4 October 1991, Dredging Research Program Technical Report DRP 92–7. U.S. USAE Waterways Experiment Station, Coastal Engineering Research Center, Vicksburg, MS, 39180–6199. http://hdl.handle.net/11681/4612.

Trincardi, F., Correggiari, A., Field, M.E., Normark, W.R., 1995. Turbidite deposition from multiple sediment sources: Quaternary Paola Basin (Eastern Tyrrhenian Sea). J. Sediment. Res. 65 (4b), 469–483. https://doi.org/10.1306/D4268289-2B26-11D7-8648000102C1865D.

Trincardi, F., Foglini, F., Verdicchio, G., Asioli, A., Correggiari, A., Minisini, D., Piva, A., Remia, A., Ridente, D., Taviani, M., 2007a. The impact of cascading currents on the Bari Canyon System, SW-Adriatic margin (Central Mediterranean). Mar. Geol. 246 (208–230), 2007. https://doi.org/10.1016/j.margeo.2007.01.013.

Trincardi, F., Verdicchio, G., Miserocchi, S., 2007b. Seafloor evidence for the interaction between cascading and along-slope bottom water masses. J. Geophys. Res. 112 (F3), F03011. https://doi.org/10.1029/2006JF000620.

Turchetto, M., Boldrin, A., Langone, L., Miserocchi, S., Tesi, T., Foglini, F., 2007. Particle transport in the Bari Canyon (Southern Adriatic Sea). Mar. Geol. 246 (2–4), 231–247. https://doi.org/10.1016/j.margeo.2007.02.007.

Verdicchio, G., Trincardi, F., 2006. Short-distance variability in slope bed-forms along the Southwestern Adriatic margin (Central Mediterranean). Mar. Geol. 234, 271–292. https://doi.org/10.1016/j.margeo.2006.09.007.

Verdicchio, G., Trincardi, F., Asioli, A., 2007. Mediterranean bottom-current deposits: an example from the Southwestern Adriatic Margin. Geol. Soc. Lond. Spec. Publ. 276, 199–224. https://doi.org/10.1144/GSL.SP.2007.276.01.10.Wade.

Wade, I.P., Heywood, K.J., 2001. Acoustic backscatter observations of zooplankton abundance and behaviour and the influence of oceanic fronts in the Northeast Atlantic. Deep-Sea Res. II Top. Stud. Oceanogr. 48 (4–5), 899–924. https://doi.org/10.1016/S0967-0645(00)00113-2.

Wåhlin, A., 2002. Topographic steering of dense bottom currents with application to submarine canyons. Deep-Sea Res. I 49 (2), 305–320. https://doi.org/10.1016/S0967-0637(01)00058-9.

Wilson, P.A., Roberts, H.H., 1995. Density cascading; off-shelf sediment transport, evidence and implications, Bahama Banks. J. Sediment. Res. 65 (1a), 45–56. https://doi.org/10.1306/D426801D-2B26-11D7-8648000102C1865D.

Xu, J.P., Noble, M., Eittreim, S.L., Rosenfeld, L.K., Schwing, F.B., Pilskaln, C.H., 2002. Distribution and transport of suspended particulate matter in Monterey Canyon, California. Mar. Geol. 181, 215–234. https://doi.org/10.1016/S0025-3227(01)00268-7.

Yuan, Y., Wei, H., Zhao, L., Jiang, W., 2008. Observations of sediment resuspension and settling off the mouth of Jiaozhou Bay, Yellow Sea. Cont. Shelf Res. 28, 2630–2643. https://doi.org/10.1016/j.csr.2008.08.005.